Reconfigurable Radio Frequency (RF) Front-end and its Fast Optimization for Adapting to Dynamic Communication Environments

Submitted in partial fulfillment of the requirements for

the degree of

Doctor of Philosophy

in

Electrical and Computer Engineering

Minhee Jun

B.S., Electrical and Computer Engineering, Mathematics (double-majored),
Korea Advanced Institute of Science and Technology
M.S., Electrical and Computer Engineering, Purdue University

Carnegie Mellon University
Pittsburgh, PA

August, 2016

I dedicate this thesis to my family members who have been so supportive for all my life: my mother Yookyung, my sister Yoonhee, and my father Inhyo in heaven.

Acknowledgments

This thesis is sponsored by the DARPA RF-FPGA (Radio Frequency-Field Programmable Gate Arrays) program under Grant HR0011-12-1-0005. The views expressed are those of the authors and do not reflect the official policy or position of the Department of Defense or the U.S. Government.

First and foremost I would like to express gratitude to my advisor, Professor Rohit Negi. I am fortunate to have been his student for my doctoral work. He has been an exemplary role model for me to learn how to think in an insightful way and predict results in a logical matter. I respect his support and advices for his students and his thoughtful sincerity. I deeply appreciate what I have learned as his student.

I would also like to thank my thesis committee: Professor Tamal Mukherjee, Professor Pulkit Grover, and Dr. Anand Dabak. Particularly, Professor Tamal has lead and contributed to this research project team of reconfigurable RF front-ends for the last four years. Also, I would like to express my appreciation to the graduate students who have dedicated their efforts to the project team: Ying-Chih Wang, Shihui Yin, and Fa Wang.

Also, I like to thank my lab colleagues, office mates and friends. Particularly, I would like to appreciate Anjali Menon, Niranjini Rajagopal, Rozana Hussin, and Ashwini Rao.

Finally, I appreciate the great teachers and professors I have previously met for the last 20 years.

Abstract

In order to support a multi-standard platform using a Software Defined Radio (SDR), the novel idea of reconfigurable Radio Frequency (RF) front-ends have recently been proposed by the U.S. Defense Advanced Research Projects Agency (DARPA). A reconfigurable RF front-end has RF components that are reconfigured separately in order to satisfy the requirement of a particular communication standard. The reconfigurable RF front-end is a more reliable front-end for SDR than the currently used fixed wide-band RF front-ends, which have degraded system performance by passing more interference signals spread out in a wide range of frequency band.

In order to realize the reconfigurable RF front-end, this thesis investigates the optimization method to select from the available configurations in radio environments with interference. In order to select an optimal configuration, we propose the Environment-Adaptable Fast (EAF) optimization algorithm for a reconfigurable RF front-end. A reconfigurable RF front-end not only needs to select an appropriate configuration that can operate for a given standard, but also needs to adapt quickly to a dynamic communication condition. This is difficult since there may be millions of available configurations. First, we studied RF impairment estimation for reconfigurable RF front-ends. Nonlinearity, phase noise, noise figure as well as frequency offset are RF impairments most likely to affect a particular standard. Second, we formulated the Signal-to-Interference-and-Noise Ratio (SINR) calculation which hastens the optimization process. We demonstrate the performance of the EAF optimization method in an exemplary scenario using Matlab Simulink. Finally, we designed the EAF optimization algorithm as a heuristic to select a configuration from the available ones. These simulation results demonstrate that while finding an optimal configuration, the EAF optimization significantly reduces simulation time compared to the four other previously proposed optimization methods. Thus, we expect that a reconfigurable RF front-end would be useful in real-time communication environments, since it would need significantly fewer reconfigurations to find an adequate configurations.

Contents

List of Figures

List of Tables

List of Algorithms

Chapter 1

Introduction

1.1 RF Front-ends in Radios

Traditionally, when multiple fixed narrow-band Radio Frequency (RF) front-ends are used for communication systems, each front-end is designed for a single communication standard as shown in Figure 1.1(a). However, the plethora of communication standards cannot be handled by the limited resources of the frequency spectrum. In order to utilize frequency spectrum efficiently, the communication standards must be handled by modern radio receivers. Frequency bands that are unused in time and space - White space - can be accessed (flexibility) and utilized by cognitive radio. Recently, multi-standard radio receivers have become important for future wireless communication systems.

In order to meet the emerging needs of multi-standard platforms, Software Defined Radio (SDR) architectures have been proposed. A fixed wide-band RF front-end is commonly used in SDR, so as to cover multiple bands of interest, as shown by Figure 1.1(b). (This particular architecture of the wideband RF front-end is based on the popular USRP SDR [14].) Flexibility in such a front-end is obtained by changing the operating fre-

quency of the local oscillator used for mixing from tens of MHz to a few GHz. In order to support operation over this large range of frequencies, this front-end uses wide-band amplifiers and mixers in a homodyne architecture, depicted in Figure 1.2(a), depending on which RF daughter-board is chosen for the SDR.

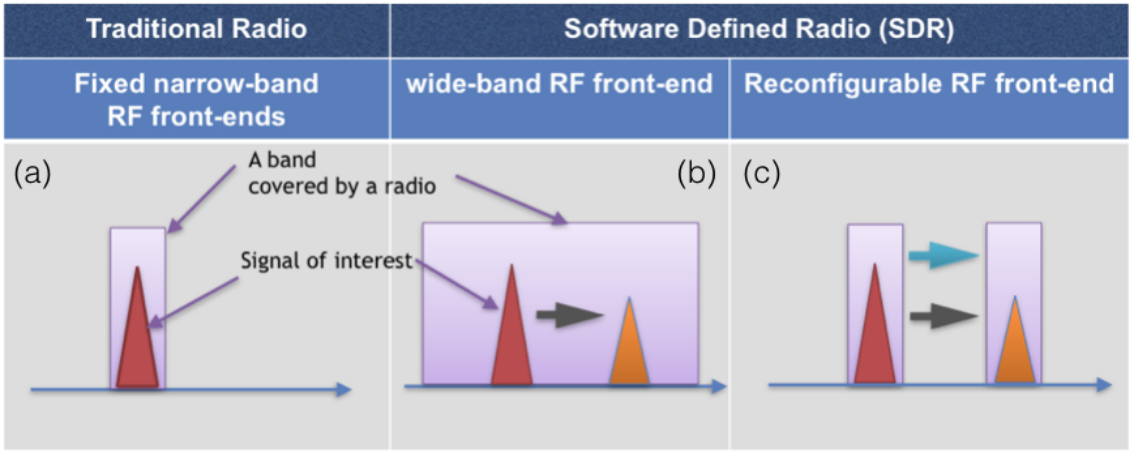

Figure 1.1: Operating frequency bands of (a) narrow-band fixed RF front-end, (b) wide-band fixed RF front-end and (c) reconfigurable (narrow-band) RF front-end. An analog-to-digital converter and a digital front-end is retained in SDR.

However, this front-end precludes the use of narrow-band RF filters [3], so that the signal of interest becomes vulnerable to inter-modulated signals. This phenomenon occurs when two or more large interferers lying outside the channel of the signal of interest, produce *in-channel interference*, due to non-linearity of the components in the wide-band RF front-end. In a typical radio receiver, there may be several large interferers - not just in the band of interest, but even far from the band of interest due to the wide-band nature of the front-end. That can cause inter-modulation interference to the desired signal.

The U.S. Defense Advanced Research Projects Agency (DARPA) has recently proposed the novel concept of a reconfigurable RF front-end (also called reconfigurable Radio Frequency-Field Programmable Gate Array (RF-FPGA)), in which various types of

RF components (conceivably arranged in component banks), may be used to select different architectures, including heterodyne and homodyne, dynamically [4]. The reconfigurable RF front-end can flexibly change its operating channel based on the requirements of the communication standard it is implementing as shown in Figure 1.1(c). Further, amplifiers, filters, and mixers in each stage can be reconfigured according to the chosen architecture and standard in Figure 1.2(b). This increases reusability of the RF components, and allows novel architectures in the RF front-end. While a fixed RF front-end is substituted with a reconfigurable RF front-end, an analog-to-digital converter and a digital front-end is retained in SDR.

Unlike the fixed wide-band RF front-end, in a reconfigurable RF front-end of SDR, RF filters can attenuate the power of large interferers, without compromising the receiver sensitivity by attenuating the signal of interest. These RF filters can alleviate the intermodulated interference, thus improving the SINR. Furthermore, appropriate choices of amplifiers and mixers can also be made to achieve the correct trade-off between sensitivity and selectivity, depending on the dynamic environment. This improvement of a reconfigurable RF front-end will be demonstrated by comparing its performance with a fixed wideband RF front-end in Appendix A. Thus, it is a promising alternative to the fixed wideband or specified narrowband front-ends used in SDRs presently.

1.2 Reconfigurable RF Front-end Optimization

With a reconfigurable RF front-end, an important challenge is finding an optimal configuration for a particular communication standard in a given RF environment. Recently, Jun Tao's study [19] investigated reconfigurable RF front-ends for radio receivers, and proposed a method to find the optimal configuration, to minimize receiver power while

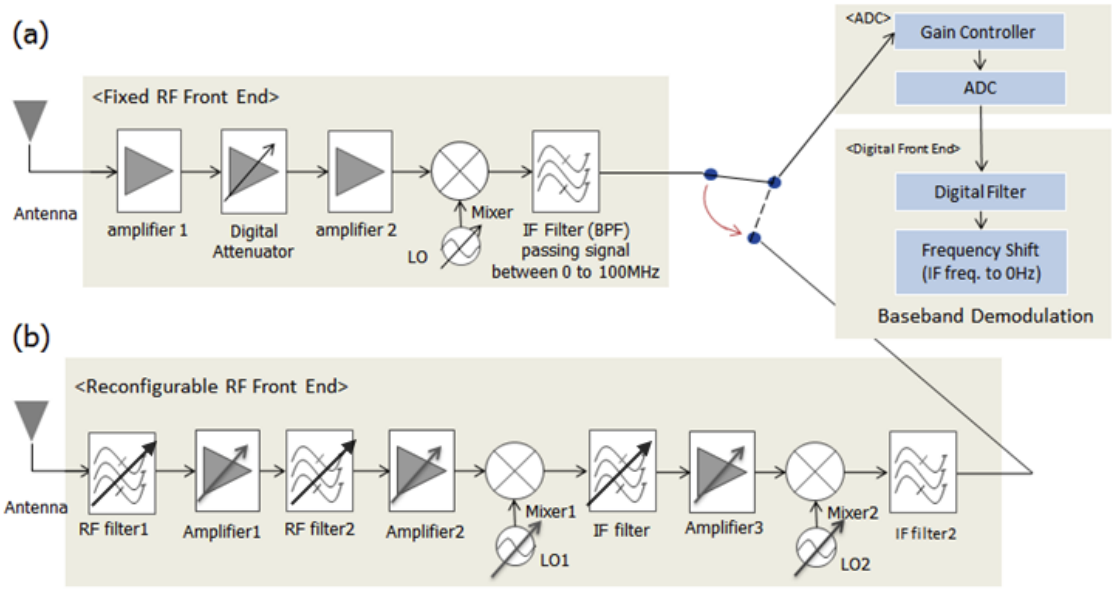

Figure 1.2: Architectures of (a) wide-band fixed RF front-end and (b) reconfigurable (narrowband) RF front-end

yielding adequate Signal-to-Noise Ratio (SNR), in a fixed communication environment. In that method, a greedy algorithm is applied to select the RF components from among those available in the RF front-end, while enforcing the minimum SNR criterion. While those results provide a starting point for our study, they do not specify how to adapt the RF front-end to a *changing RF environment* - specifically to the appearance of large interferers and blockers. In the presence of interference, the optimal configuration is one which has the lowest power consumption and adequate quality of communication as measured by the Signal-to-Interference-and-Noise Ratio (SINR). This reconfiguration must be done quickly, by efficiently exploring space of millions of likely configurations.

To find an optimal configuration $\mathbf{x}^{(opt)}$ of the reconfigurable RF front-end, the optimization problem can be mathematically formulated as follows,

$$\begin{aligned} \mathbf{x}^{(opt)} = \quad & arg\min \quad F(\mathbf{x}), \\ & g_i(\mathbf{x}, t) \geq G_i \quad \forall i \in \{1, 2, \cdots, N_g\} \end{aligned} \tag{1.1}$$

where the vector-valued $\mathbf{x}$ is one of the available configurations for a reconfigurable RF front-end and each element of $\mathbf{x}$ is a parameter of an individual component. $F(\mathbf{x})$ is a cost function (such as power consumption of the configuration), which needs to be minimized while satisfying all constraints $g_i(\mathbf{x}, t) \geq G_i$ for $i \in \{1, 2, \cdots, N_g\}$ at time t (signal-to-interference-plus-noise ratio, area, cost, etc.).

The main difficulty in finding the optimal configuration is the adaptation complexity, measured in the time needed to discover the optimal configuration, due to the exponential number of possible configurations when the number of RF components (amplifiers, filters, and mixers) is large, and when there are several stages of RF signal processing. When the reconfigurable radio is initially programmed, several base configurations (i.e., default configurations) can be pre-programmed into it, based on the desired communication standards. However, the spectral environment is dynamic, with blockers and large interferers appearing randomly at different frequencies. This cannot be pre-programmed exhaustively, since there are too many possible scenarios to be considered. Rather, a fast algorithm to adapt the RF front-end to interferers in real-time is needed.

1.3 Environment-Adaptable Fast Optimization Method

In this thesis, we developed a fast optimization algorithm - called Environment-Adaptable Fast (EAF) optimization - for optimizing a reconfigurable RF front-end in a dynamic spectrum environment. We improve the efficiency of an optimization method by predicting configurations that can be discarded, based on Signal-to-Interference-and-Noise Ratio (SINR), which is *calculated* -as opposed to simulated (or measured during operation)- using RF impairment information. Our contributions to reconfigurable RF front-end optimization are given below:

First, we estimated RF impairments of a reconfigurable RF front-end (in Chapter 2). To conduct this estimation, we designed estimators for Time-Invariant (TI) Impairments, including nonlinearity, phase noise and noise figure, and Time-Variant (TV) impairments, including frequency offset.

Second, utilizing the estimated RF impairments, we designed the EAF optimization method that improves optimization speed by utilizing the calculated SINR (in Chapter 3). The calculated SINR was formulated in terms of parameters of RF impairments and signal spectrum of the signal of interest and interferers. The performance of the EAF optimization was demonstrated in a reconfigurable RF-FPGA system.

Finally, the EAF optimization method was expanded and applied to a large-scale reconfigurable RF-FPGA system (in Chapter 4). In a large-scale RF front-end, the main problem is that the RF impairments of all possible configurations cannot be estimated due to the large number of possible configurations. Our approach for this problem was to model the RF front-end in terms of component values, and to estimate the component parameters using a Design of Experiments approach and an Interpolation method. This thesis extensively uses simulations to model and verify the system and algorithm. This is done using Matlab Simulink, augmented with the SimRF toolbox. Simulink can model the baseband of a communication system in detail. The SimRF toolbox is capable of modeling RF operations, such as filtering, mixing, and amplification, including detailed noise, nonlinearity and frequency response modeling.

1.4 Our Contributions

This thesis claims the following novel contributions,

1. We studied RF impairment estimation for a large-scale RF-FPGA system. We

derived statistical signal models of RF impairments, and based on the statistical signal models we designed estimators of RF impairments. We focused on two main problems while applying the estimators of RF impairments to a large-scale RF-FPGA system: two saturation areas of nonlinearity estimates and limited resources in RF impairment estimation procedures. The saturation areas of nonlinearity estimates are caused by a wide range of RF front-ends. In order to solve the saturation, we designed a formula for changing the transmission signal power in an estimation procedure. Also, we considered limited resources in RF impairment estimation in a large-scale RF front-end. Solving the limited resource problem, we used a Design of Experiments (DoE) approach that effectively selects sample configurations among the large number of all possible configurations in a large-scale RF-FPGA and an Interpolation method that obtains unknown component values from known component values of RF impairments calculated from sample configurations.

2. We derived a formula that calculates SINR in a given communication environment in terms of phase noise, nonlinearity and noise figure. In order to improve the accuracy of the SINR calculation, the impairing signal power by each RF impairment was separately analyzed considering the frequency offset of interference and the power of the signal of interest and interference. We assumed that RF impairments are estimated, and a signal spectrum is obtained by a Signal Analyzer, a configuration of reconfigurable RF front-ends that bypasses all filters and amplifiers.

3. Using the SINR calculation, we designed the EAF optimization method that hastens an optimization process for finding an operable configuration in a large-scale RF-FPGA system. Simulation results showed that our EAF optimization method significantly improves its optimization speed compared with the Two-phase relaxation optimization method and the Multi-resolution optimization method.

Chapter 2

RF Impairments and Estimation

The RF signal received by a RF front-end suffers from various deleterious effects as it is processed by the RF front-end, resulting in a certain SINR at the baseband. Therefore, to calculate SINR for the EAF optimization presented in Chapter 3, we first need to estimate RF impairments of any configurations of the RF-FPGA. The relation between SNR (or BER) and RF impairment has been studied previously, for example in [11]. The estimators of RF impairments help the reconfigurable engine narrow down candidate configurations from the pool of all configurations of reconfigurable RF systems. Based on the estimates of RF impairments, configurations with dominant RF impairments can be eliminated in the pool of candidate configurations [17].

Communication standards have different requirements of RF impairments. The estimates of RF impairments of configurations directly tell us which configurations satisfy the requirements of RF impairments for a given standard. For example, the IEEE 802.11a/b/g standards require maximal gain of 18 dB, the third-order nonlinearity (IP3) of -5 dBm, noise figure of 3 dB [2]. Therefore, the estimators of RF impairments discriminate among useful configurations, and thus quicken the optimization process for reconfigurable RF front-ends for different standards.

The RF impairments to be estimated considered are chosen based on the typical baseband standard requirements from a study published by Brendolini as shown in Table 2.1: IIP3, phase noise, noise figure and gain.

RF impairments are estimated using baseband signals received after downconversion by the reconfigurable RF front-end. Baseband signals are distinctively impaired by different types of RF impairments. Also, baseband signals require a relatively lower sampling frequency (typically, only up to a few tens of MHz) than passband signals, which are typically in the GHz range.

There are two types of RF impairments: Time-Invariant (TI) RF impairments and Time-Variant (TV) RF impairments. A TI RF impairment is characterized by fixed parameters while the TV RF impairment parameters may change over time.

Considering the characteristics of TI and TV RF impairments, we investigated estimation methods for nonlinearity, phase noise, noise figure, gain, and frequency offset.

Table 2.1: Baseband Standard Requirement [2]. (phase noise is specified at 1MHz frequency offset.)

Standard	E-GSM (2G)	UMTS (3G)	802.11a/g	802.11b
f (GHz)	0.88-0.915	1.85-1.91	5.15-5.725	2.4-2.4835
Noise Figure	9 dB	6 dB	7.5 dB	14.8 dB
Phase Noise	-141 dBc/Hz	-150 dBc/Hz	-102 dBc/Hz	-101 dBc/Hz
IIP3	-18 dBm	-18 dBm	-16 dBm	-16 dBm
IIP2	+49 dBm	+46 dBm	-	-

2.1 Time-Invariant (TI) RF Impairments

Because of the fixed parameters of Time-Invariant (TI) RF impairments, it is assumed that the TI impairments - nonlinearity, phase noise and noise figure - are estimated when a reconfigurable RF front-end is manufactured, called Factory mode of operation (Appendix B).

2.1.1 Third Order Nonlinearity Estimator Design

The third order nonlinearity causes impairing received signals due to intermodulation of the signal of interest and interference. The third-order nonlinearity is generally represented by the third-order intercept point (IP_3).

In order to estimate IP_3 that is defined as $IP_3 = \sqrt{\frac{4}{3}\frac{\alpha_1}{\alpha_3}}$ where α_1 and α_3 are the first and third order gains respectively, we need to start by categorizing blockers [6].

First, set $B^{(k)}$ is defined as a set of all pairs of blockers, which may cause intermodulated signals by third order non-linearity of the k-th configuration of a reconfigurable RF front-end.

$$B^{(k)} = \{(b_m, b_n) : |2 \cdot F_m - F_n - F_c| < 0.5 \cdot \mathbf{B}\}, \tag{2.1}$$

where the two narrowband blockers b_m and b_n are located at the frequencies of F_m and F_n, respectively. F_c is the carrier frequency of the signal of interest and $\mathbf{B}$ is the bandwidth of the signal of interest. The pair of blockers b_m and b_n can be located either at the right-handed side of the carrier frequency F_c such as $F_c < F_m < F_n$ or at the left-handed side such as $F_n < F_m < F_c$ on the frequency spectrum.

Since there are N_k filters in the k-th configuration of the reconfigurable RF front-end, we can order the filters in the order in which the signal passes through the RF-FPGA chain. Suppose the passband of i-th filter is denoted by P_i. A pair of blockers (b_m, b_n) in

the set $B^{(k)}$ may or may not simultaneously pass the i-th filter (e.g., F_m and F_n may or may not in P_i) for $i \in \{1, 2, \cdots, N_k\}$.

Now, we can group pairs of blockers (b_m, b_n), into N_k subsets ${B_i}^{(k)}$ of set $B^{(k)}$ based on F_m, F_n and passband P_i of the i-th filter as follows, ${B_{N_k+1}}^{(k)} = \emptyset$ and then for $i = N_k, N_{k-1}, \cdots, N_1$, define

$$ {B_i}^{(k)} = \{(b_m, b_n) \in B^{(k)} : F_m \in \bigcap_{r=1}^{i} P_r, F_n \in \bigcap_{r=1}^{i} P_r, \quad (b_m, b_n) \notin {B_{i+1}}^{(k)}\}. \tag{2.2} $$

There is only one set ${B_i}^{(k)}, i \in \{0, 1, 2, \cdots, N_k\}$ containing a given pair of blockers

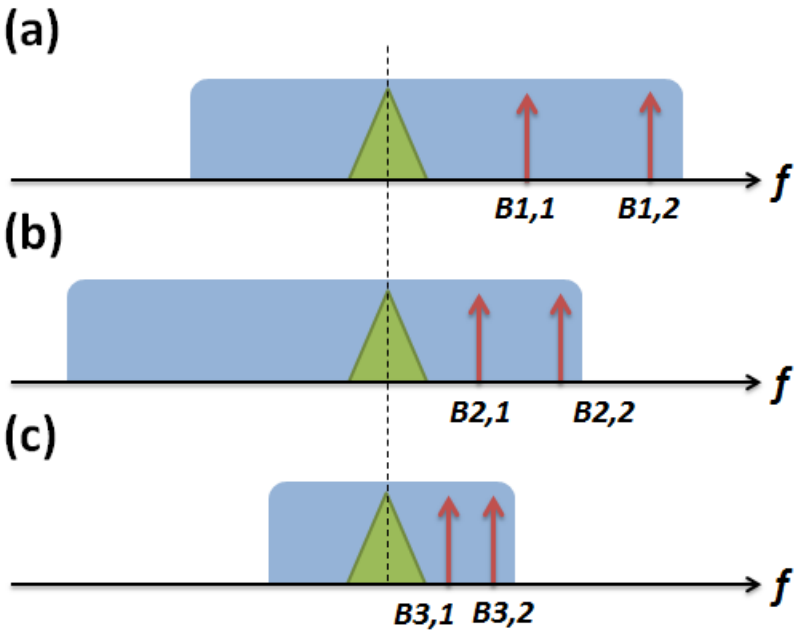

Figure 2.1: An example of categorization of a blocker pair (b_m,b_n): the k-th configuration has three RF filters (e.g. see Figure 1.1 (b) with two RF filters) with passband ranges plotted in (a), (b), and (c), respectively, in order. The first subset ${B_1}^{(k)}$ has a pair of blockers ($B_{1,1}$,$B_{1,2}$). Both of the blockers are placed in the passband (a) of the first filter but at least one of them is not in the passband (b) of the second filter. Similarly, subsets ${B_2}^{(k)}$ and ${B_3}^{(k)}$ are shown in (b) and (c) respectively.

(b_m, b_n) in $B^{(k)}$. If a pair of blockers (b_m, b_n) belongs to ${B_i}^{(k)}$, at least one of the blockers are significantly attenuated by the $(i+1)$-th filter. Then, after passing through the $(i+1)$-th filter, inter-modulation of blockers does not occur additively. In other words, the inter-modulation of blockers is caused by third order nonlinearity of RF components, through which blockers have passed before passing the $(i+1)$-th filter. Suppose parameter $\text{IP3}_{i,k}$ represents the effective IP3 of the chain of RF components through which blockers have passed before passing through the $(i+1)$-th filter in the k-th configuration. In this case, $\text{IP3}_{i,k}$ for $i \in \{1, 2, \cdots, N_k\}$ directly affects the magnitude of inter-modulated signals caused by the blocker pairs in the set of ${B_i}^{(k)}$.

In order to estimate third order nonlinearity parameter $\text{IP3}_{i,k}$, we use two sinusoidal signals belonging to the frequency band $\bigcap_{r=1}^{i} P_r$ while one of the two sinusoids does not belong to $\bigcap_{r=1}^{i+1} P_r$. Assume that when two such sinusoids of amplitude $A_{1,i,k}$ and $A_{2,i,k}$, respectively, pass through the reconfigurable RF front-end, the received inter-modulated signal has amplitude $A_{out,i,k}$. Assume that when a single sinusoid of amplitude of $B_{in,k}$ at a frequency F_s in the frequency band $\bigcap_{r=1}^{N_k} P_r$, passes through the reconfigurable RF front-end, the received signal has amplitude $B_{out,k}$.

Then, $\widehat{\text{IP3}}_{i,k}$ is given by the following formula [6],

$$\widehat{\text{IP3}}_{i,k(\text{dBm})} = -10 \cdot \log_{10}\left(\frac{A_{out,i,k}}{{A_{1,i,k}}^2 \cdot A_{2,i,k}} \frac{B_{in,k}}{B_{out,k}}\right) + 30. \tag{2.3}$$

Thus, varying the frequencies of the generated one or two sinusoids and sending the sinusoids through the reconfigurable RF system, we can obtain a set of $\widehat{\text{IP3}}_{i,k}$, where $i \in \{1, 2, \cdots, N_k\}$ of the k-th configuration.

In addition, the gain G_k of the k-th configuration is estimated by the following formula,

$$\widehat{G_{k(dB)}} = 20 \cdot log_{10}\left(\frac{B_{out,k}}{B_{in,k}}\right). \tag{2.4}$$

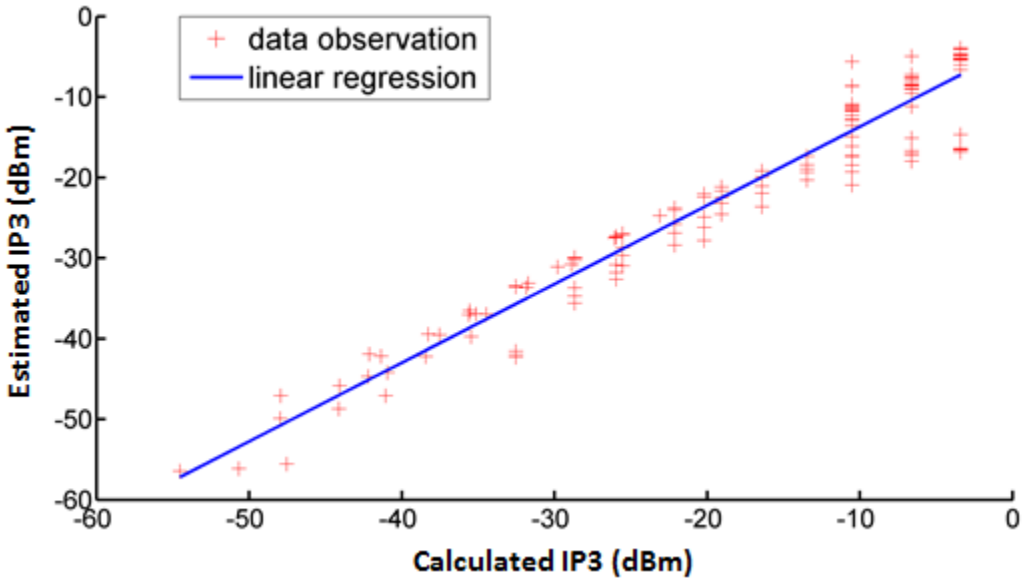

Figure 2.2: Estimated of $\text{IP3}_{i,k}$ vs. Calculated $\text{IP3}_{i,k}$ for $i = 1, 2, 3$ of the reconfigurable RF system in Fig 1.2 (b).

Simulation and Results

The system was simulated using Matlab Simulink with the SimRF toolbox, as shown in Figure 2.3 and 2.4.

The estimation result of $\text{IP3}_{i,k}$ is plotted in Figure 2.2. $\text{IP3}_{i,k}$, obtained by our estimation method in (3.6), is on the y-axis, and $\text{IP3}_{i,k}$, calculated from each IP3 and gain of amplifiers, is on the x-axis. We observe that the estimated IP3 proportionally increases with the calculated IP3. The variation between the calculated IP3 and the estimated IP3 is because the calculated IP3 on the x-axis did not account for the insertion loss of filters or the gain and the nonlinearity in mixers, while the estimated IP3 did.

Therefore, using this method we estimated the non-linear parameters $\text{IP3}_{i,k}$, and stored them in a table of RF impairments for all possible configurations in Factory mode (Appendix B).

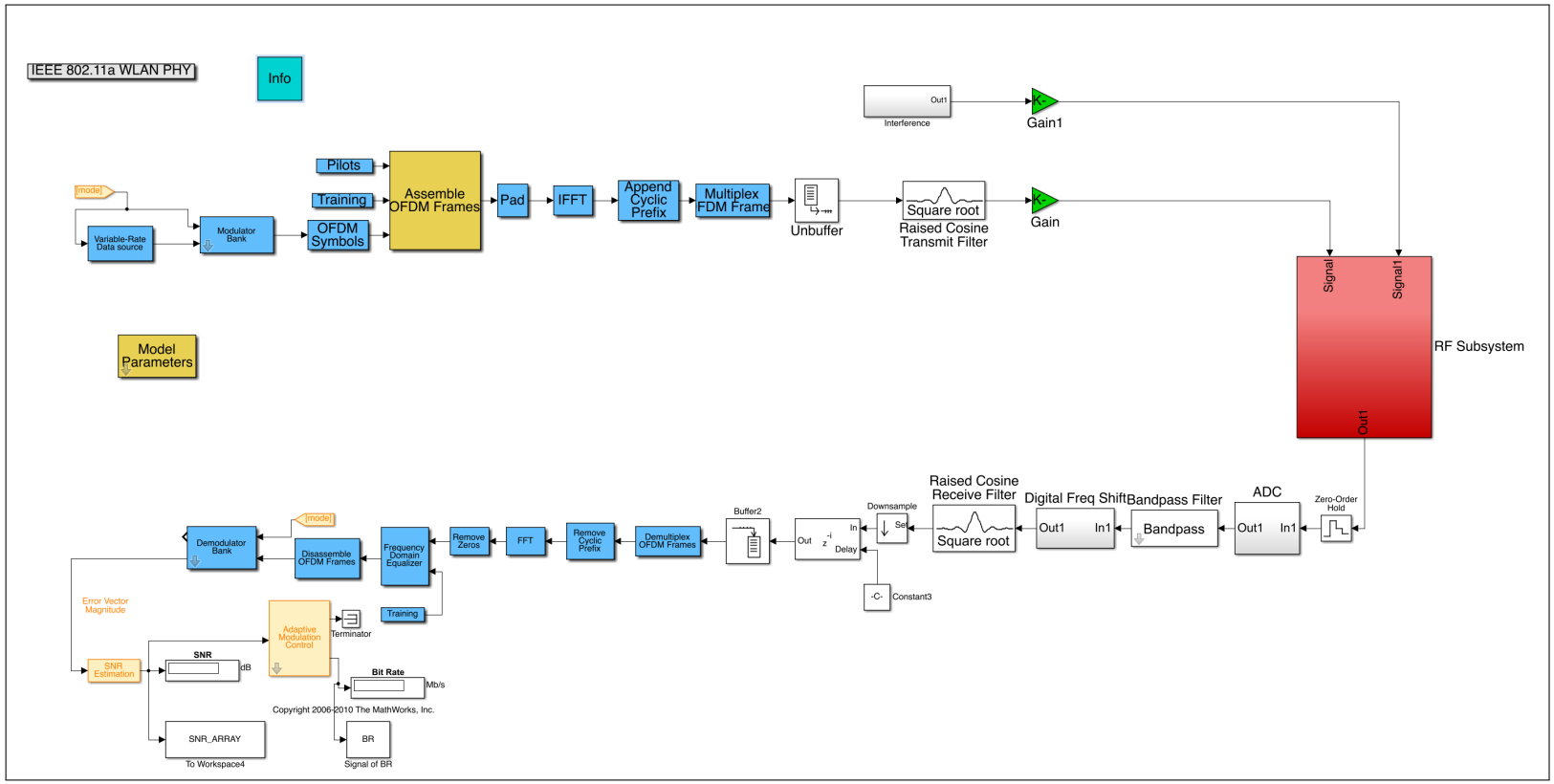

Figure 2.3: Matlab Simulink is used for implementing a communication system setting and a RF front-end system

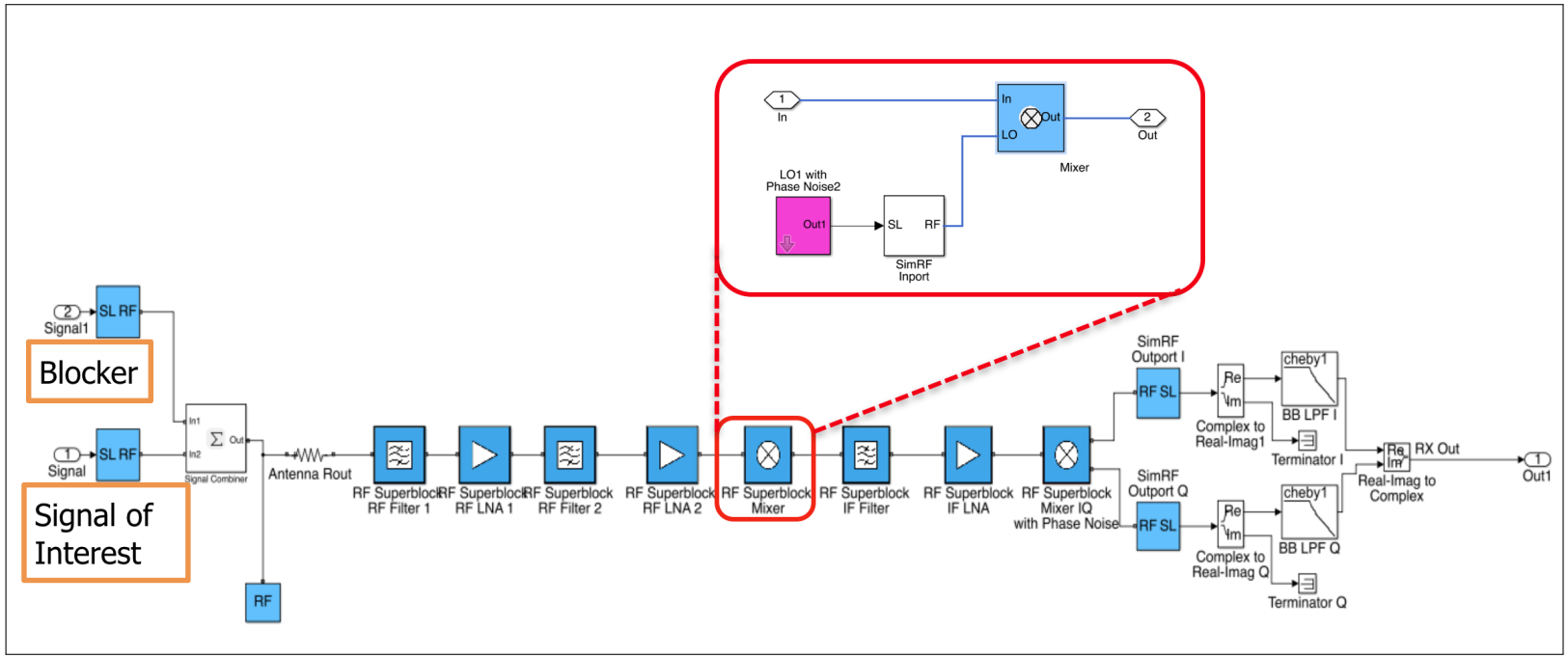

Figure 2.4: SimRF toolbox is used for the simulation setting of the RF front-end system (the red box in Figure 2.3)

2.1.2 Phase Noise Estimator Design

Phase noise is one of the most important RF impairments with respect to baseband standard requirements. Phase noise can degrade communication quality by mixing with strong unwanted signals (Appendix C).

There have been studies for modeling a stochastic process with typical phase noise spectra and generating stochastic signals caused by phase noise. The three main categories of phase noise spectrum modeling are given as (1) ARMA based models, (2) fractional integration models, (3) wavelength based models of $1/f$ noise [9]. In this thesis, the fractional integration model - the most common approximation - is applied to the model phase noise process for reconfigurable RF front-ends.

The fractional integration model is a superposition of filters with one pole that converges to the phase noise spectrum in the limit of a large number of filters. Instead of choosing the pole positions carefully, the Interpolated Finite Impulse Response (IFIR)

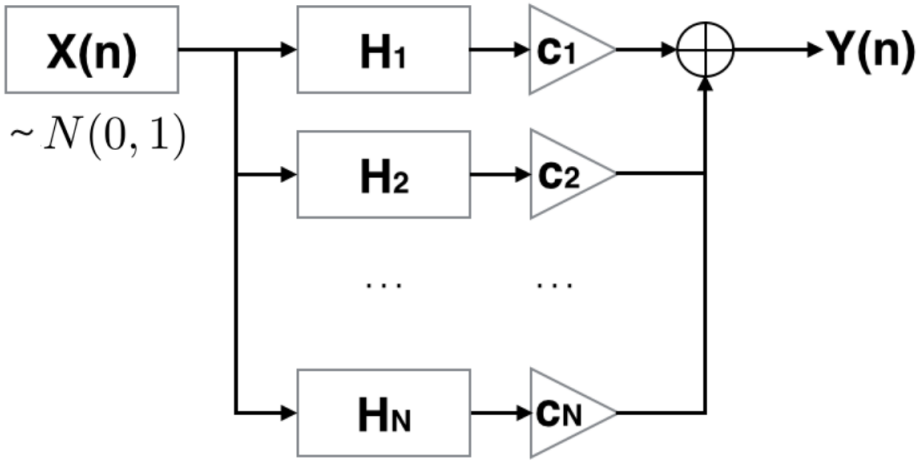

Figure 2.5: The IFIR model for phase noise spectrum estimation: the basis filters $H_1, H_2, \cdots, H_N$ are fixed, and the gains $c_1, c_2, \cdots, c_N$ are adjustable. $X(n)$ is AWGN of mean of 0 and variance of 1.

approach fixes the pole positions for basis filters and carefully chooses gains of the filters [20].

Interpolated FIR (IFIR) Model

The IFIR model in Figure 2.5 has the fixed basis filters $H_1, H_2, \cdots, H_N$ and the adjustable gains $c_1, c_2, \cdots, c_N$. The discrete time sequence (X_n) is Additive White Gaussian noise (AWGN) of mean of 0 and variance of σ_n^2.

The IFIR model can efficiently describe phase noise spectrum as the weighted sum of lower order basis filters [13]. Assume that there are N basis filters, with a frequency response of $H_1, H_2, \cdots, H_N$. We define the transition bandwidth of H_k, $(\omega_p^{(k)}, \omega_s^{(k)})$ such that $\omega_s^{(k)} = M\omega_p^{(k)} = \omega_p^{(k+1)}$, where M is a constant that determines the bandwidth size of H_k. The highest frequency should be smaller than half of the sampling frequency, $\omega_s^{(N)} < F_s/2$ where F_s is the sampling frequency. The transition bandwidth of H_k is given as follows,

$$(\omega_p^{(k)}, \omega_s^{(k)}) = M^{k-1} \cdot (\omega_p^{(1)}, \omega_s^{(1)}). \tag{2.5}$$

Then, the filters H_k are designed using Algorithm 1 [8].

Algorithm 1 The Basis Filter Design Algorithm

1: **Generate a digital lowpass filter** $G(e^{j\omega})$ **with transition bandwidth** $(\omega_p^{(N)}, \omega_s^{(N)})$
2: $H_N(e^{j\omega}) = G(e^{j\omega})$
3: **for** $k = 1, 2, \cdot, N-1$ **do**
4: **filter** $G_k(e^{j\omega}) = G(e^{jM^{N-k}\omega})$
5: **lowpass filter** $I_k(e^{j\omega})$ **with stop frequency** $\omega_s^{(N)}/M^{N-k}$
6: **filter** $H_k(e^{j\omega}) = G_k(e^{j\omega})I_k(e^{j\omega})$
7: **end for**
8: **Return** $H_1(e^{j\omega}), H_2(e^{j\omega}), \cdots, H_k(e^{j\omega}), \cdots, H_N(e^{j\omega})$.

The IFIR design algorithm efficiently reduces the order of designed basis filters. The Bode plots of some of the filters in Algorithm 1 are illustrated in Figure 2.6. We first

implemented the digital filter $G_k(e^{j\omega})$ in line 1 using a Butterworth low-pass filter with a passband attenuation of 1 dB and a stopband attenuation of 20 dB. We set $M = 2$ and $N = 13$. In line 4, $G_k(e^{j\omega}) = G(e^{jM^{N-k}\omega})$ was obtained by up-sampling the time domain signal $g_k(t) = FT^{-1}(G_k(e^{j\omega}))$ with the up-sampling factor M^{N-k} (the function FT^{-1} is the inverse Fourier transform). Then, the lowpass filter $I_k(e^{j\omega})$ eliminates the replicas in $G_k(e^{j\omega})$ obtained due to up-sampling.

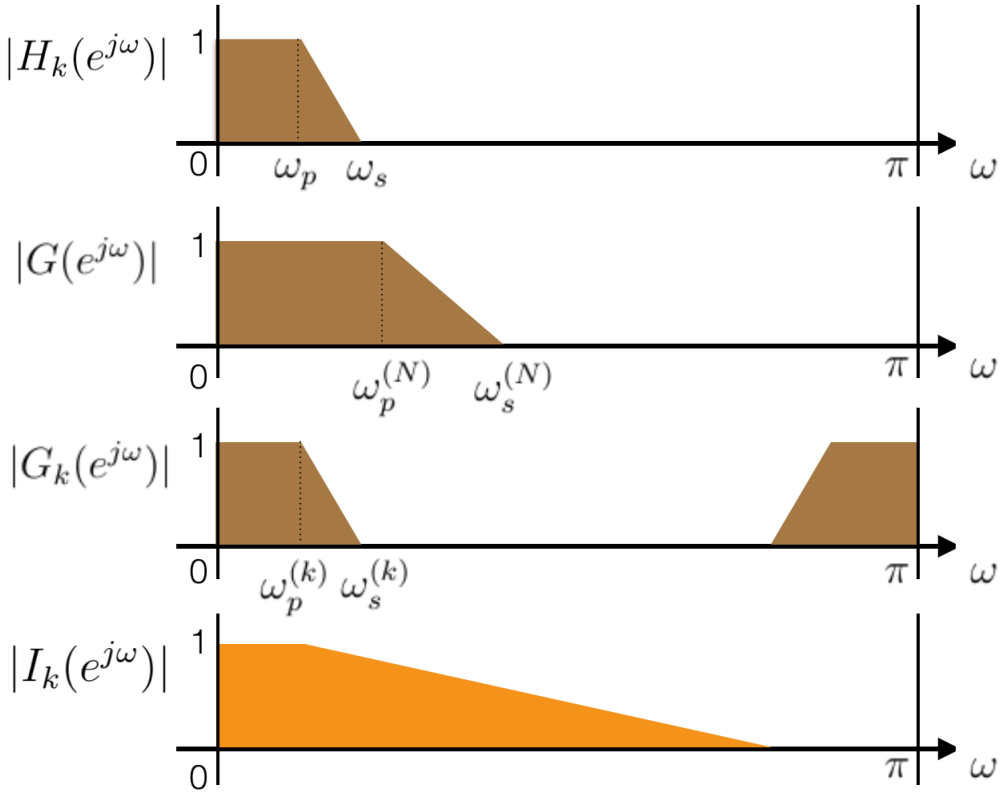

Figure 2.6: Filters described in Algorithm 1.

Statistical Signal Model and Estimation of Phase Noise

While the IFIR technique was previously implemented in a heuristic manner in [13], we establish a rigorous statistical signal model for utilizing the IFIR model. Then, we

derive an estimator for the phase noise spectrum and apply the Least Mean Squares (LMS) adaptive algorithm to complete the estimator.

Statistical Signal Model The signal subspace model is defined as follows [15],

$$Y = X \bullet H_C + N, \tag{2.6}$$

where Y, X, H_C, N are $M \times 1$ vectors. Y is a vector of a received signal in the frequency domain, X is a vector of a AWGN in the frequency domain, and N is a vector of AWGN, measurement noise. $H_C(f_k) = c_1 H_1(f_k) + c_2 H_2(f_k) + \cdots + c_N H_N(f_k)$ is the frequency response of the IFIR model in Figure 2.5, where the vector H_i is the frequency response of the i-th basis filter in the frequency domain and the variable c_i is a gain. The '$\bullet$' operator is the element-wise product. Since the basis filters $H_i(f)$ are fixed, only the gains c_i need to be estimated.

Then, the k-th element Y_k of the vector Y is,

$$Y_k = Y(f_k) = X(f_k) \cdot H_C(f_k) + N(f_k), \tag{2.7}$$

where $Y(f_i)$ and $Y(f_j)$ are independent if $i \neq j$, and $Y(f_k) \sim N(0, 1 \cdot |H_C(f_k)|^2 + {\sigma_n}^2)$ for $k = 1, 2, \cdots, M$.

Problem Definition and Maximum Likelihood Estimator (MLE) We need to obtain the gains $c_1, c_2, \cdots, c_N$ for the given model in Figure 2.5. While the variance σ_n^2 can also be estimated, we found that we can typically set it to 0.

We define the vector $C = [c_1, c_2, \cdots, c_N]^T$. Then, the log-likelihood function $L(C, Y)$ of the vector Y is,

$$\begin{aligned} L(C,Y) &= ln f_C(Y) = ln \prod_{f_k} f_C(Y(f_k)) = \sum_{f_k} ln f_C(Y(f_k)) \\ &= \frac{1}{2} \sum_{f_k} \left(-ln|H_C(f_k)|^2 - \frac{|Y(f_k)|^2}{|H_C(f_k)|^2} \right) + \text{const.}, \end{aligned} \tag{2.8}$$

assuming $\sigma_n^2 = 0$.

The maximum likelihood estimator (MLE) $\widehat{C}$ is obtained by maximizing the log-likelihood $L(C, Y)$.

$$\widehat{C} = \max_C L(C, Y). \tag{2.9}$$

In order to prevent overfitting the vector C, we added the Lasso regularization $||C||_1 = \sum_k |c_k|$ in (2.9).

$$\begin{aligned} \widehat{C} &= \max_C L(C, Y) - \gamma \cdot ||C||_1 \\ &= \max_C \frac{1}{2} \sum_{f_k} \left(-ln|H_C(f_k)|^2 - \frac{|Y(f_k)|^2}{|H_C(f_k)|^2} \right) - \gamma \cdot ||C||_1. \end{aligned} \tag{2.10}$$

Defining the cost function $J(C) = -(L(C, Y) - \gamma \cdot ||C||_1)$, we can rewrite (2.10) in a way of minimizing $J(C)$,

$$\begin{aligned} \widehat{C} &= \min_C J(C) \\ &= \min_C \frac{1}{2} \sum_{f_k} \left(ln|H_C(f_k)|^2 + \frac{|Y(f_k)|^2}{|H_C(f_k)|^2} \right) + \gamma \cdot ||C||_1. \end{aligned} \tag{2.11}$$

Because of complications - dealing with the **complex** estimator $\widehat{C}$, we applied the LMS adaptive algorithm.

The two main modifications from the primary LMS adaptive algorithm are initialization and termination: (1) The initialization condition in line 2 is modified from $C^{(0)} = 0$ to $C^{(0)} = (H^T H)^{-1} H^T Y_a$ where $(Y_a)_k = |(Y)_k|$. This modification prevents the metric Δ_i in line 13 from being ∞ at the first iteration, and it also reduces the convergence time for the while loop. (2) The termination condition is modified from estimator error convergence to spectrum error convergence. Without the modification, the estimator error convergence condition suffers from convergence to a local optimum depending on the initial point $C^{(0)}$.

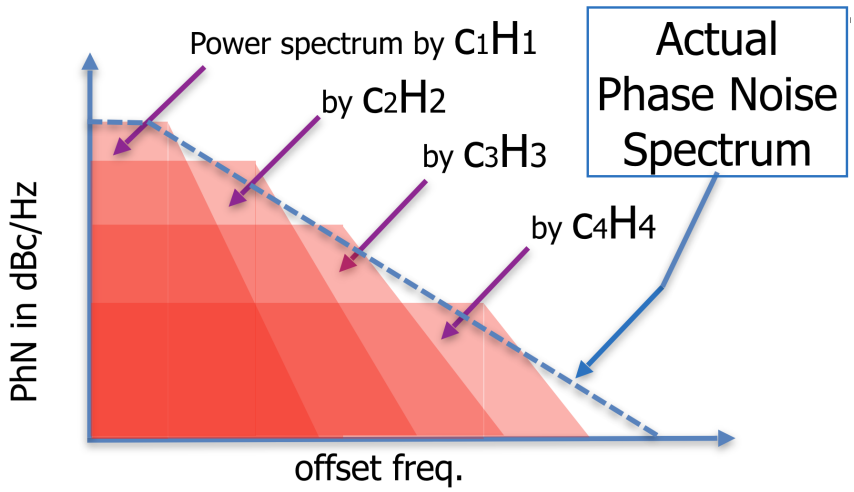

Figure 2.7: A phase noise power spectral density can be calculated as $L(f) = |H_C(f)|^2 = |c_1H_1(f) + c_2H_2(f) + \cdots + c_mH_m(f) + \cdots + c_NH_N(f)|^2$.

Applying the LMS adaptive algorithm, we need the metric Δ_i, the derivative of $J(C)$ in terms of c_i,

$$\Delta_i = \frac{dJ(C)}{dc_i} \tag{2.12}$$

$$= \frac{1}{2}\sum_{f_k} \frac{H_i(f_k)}{H_C(f_k)} \left(1 - \frac{|Y(f_k)|^2}{|H_C(f_k)|^2}\right) + \gamma \cdot sign(c_i). \tag{2.13}$$

Therefore, we update the i-th element c_i of the vector C iteratively as follows,

$$c_i^{(k+1)} = c_i^{(k)} - \mu \cdot \Delta_i, \quad i = 1, 2, \cdots, N, \tag{2.14}$$

for $k \geq 1$ and the step size μ.

We applied the LMS adaptive algorithm to do the optimization. Then, the phase noise power spectral density can be calculated as $L(f) = |H_C(f)|^2 = |c_1H_1(f) + c_2H_2(f) + \cdots + c_mH_m(f) + \cdots + c_NH_N(f)|^2$ in Figure 2.7.

The pseudocode of the LMS adaptive algorithm is given in Algorithm 2.

Algorithm 2 The LMS Adaptive Algorithm for obtaining $\widehat{C}$.

$\epsilon = \epsilon_0$, $\mu = \mu_0$, $\gamma = \gamma_0$
$C^{(0)} = (H^T H)^{-1} H^T Y$ where $H = [H_1, H_2, \cdots, H_N]$
$c_m^{(0)} = (C^{(0)})_m$ for $m = 1, 2, \cdots, N$.
$k = 0$
while $k \leq k_{max}$ **do**
    $H_C = c_1^{(k)} H_1 + c_2^{(k)} H_2 + \cdots + c_m^{(k)} H_m + \cdots + c_N^{(k)} H_N$
    if $k > 0$ **then**
        $e = \text{var}(|Y - H_C|)$
        if $e < \epsilon$ **then**
            break
        end if
    end if
    $\Delta_m = \frac{1}{2} \sum_{f_k} \frac{H_m(f_k)}{H_C(f_k)} \left(1 - \frac{|Y(f_k)|^2}{|H_C(f_k)|^2}\right) + \gamma \cdot sign(c_m)$
    for $m = 1, 2, \cdots, N$ **do**
        $c_m^{(k+1)} = c_m^{(k)} - \mu \cdot \Delta_m$
    end for
    $C^{(k+1)} = [c_1^{(k+1)}, c_2^{(k+1)}, \cdots, c_N^{(k+1)}]$
    $k \leftarrow k + 1$
end while
return $\widehat{C} = C^{(k)}$

Simulation and Results

Simulation results of phase noise estimation using Algorithm 2 are plotted in Figure 2.8. A phase noise power spectral density $L(f)$ for a given phase noise is plotted in Figure 2.8a. We applied Algorithm 2 to obtaining gains c_k, and obtained the phase noise power spectral density $L(f)$ using a formula $L(f) = |H_C(f)|^2 = |c_1 H_1(f) + c_2 H_2(f) + \cdots + c_m H_m(f) + \cdots + c_N H_N(f)|^2$. In the plot, the obtained phase noise spectral density (red) described the characteristic of the given phase noise (blue) in an acceptable range. The Root-Mean-Square Error (RMSE) of the estimated phase noise is plotted against the true phase noise (dBc/Hz) at 1 MHz frequency offset in Figure 2.8b. The oscillator in our simulation has five configurations: $-102, -104, -108, -118, -123$ dBc/Hz at 1 MHz offset frequency. The NMSE shows that the LMS adaptive algorithm provides estimates of phase noise within an acceptable range.

2.1.3 Noise Figure Estimator Design

An ideal RF receiver has AWGN of power $kT\mathbf{B}$ where k is the Boltzmann constant, T is temperature, and $\mathbf{B}$ is the total bandwidth. In an actual receiver, additional noise is caused by RF components such as amplifiers, and is represented by a noise figure.

Noise figure is estimated using the invariant estimator design that is explained in Section 2.2. So, we defer its description to Section 2.2.2.

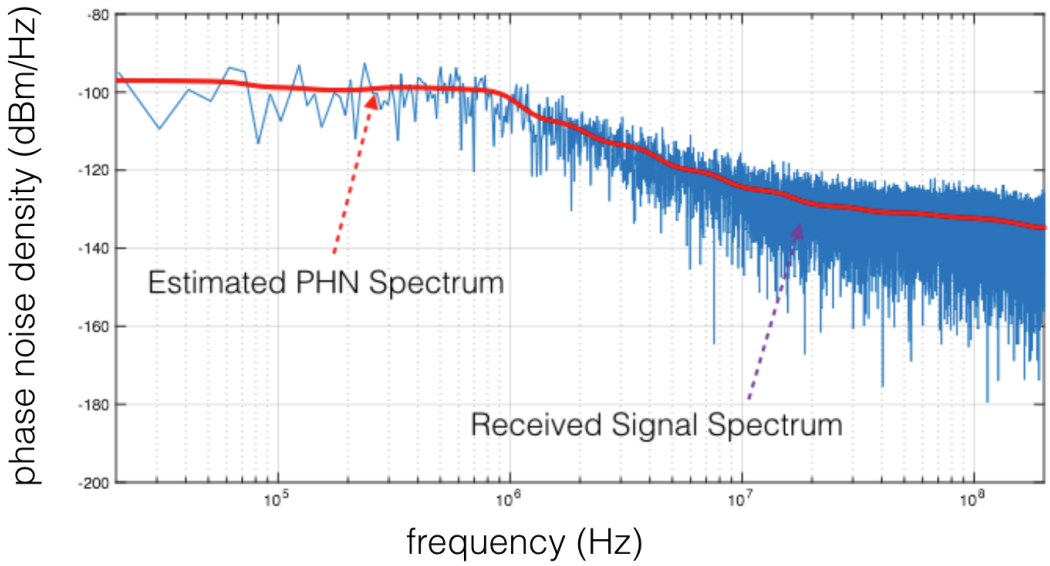

(a) An estimated phase noise spectrum density $L(f)$ in dBc/Hz (red) for the given phase noise (blue). Frequency on the x-axis is log-scaled.

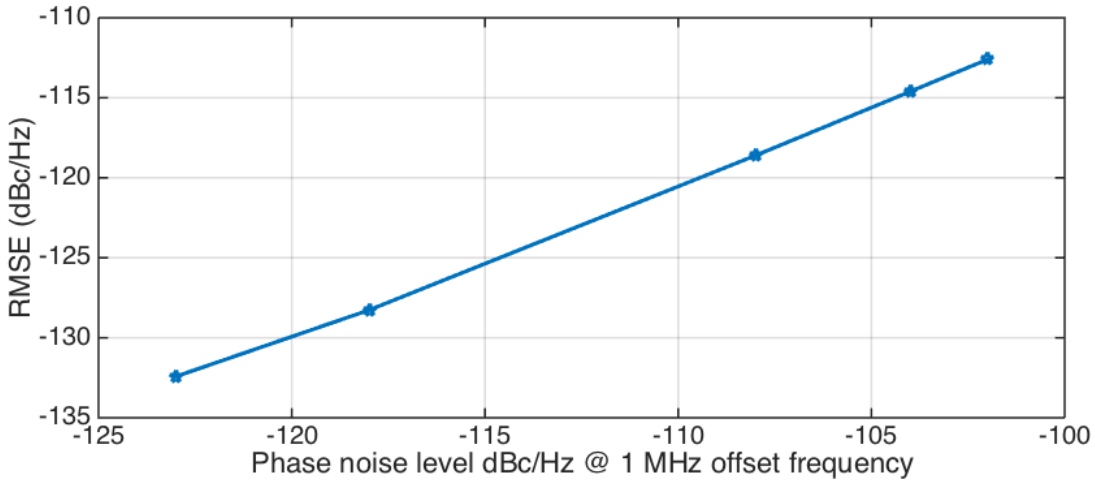

(b) The RMSE of the estimated phase noise (dBc/Hz at 1MHz frequency offset) vs. true phase noise (dBc/Hz at 1MHz frequency offset).

Figure 2.8: Simulation results of the estimated phase noise.

2.2 Time-Variant (TV) RF Impairments

Time-Variant (TV) RF impairments need to be periodically estimated and updated using pilot signals because of its dynamic characteristic. In order to estimate TV RF impairments efficiently, joint invariant estimators are derived based on a signal subspace model [7].

The frequency offset impairment, an example of TV RF impairment, represents the time-varying mismatch of the carrier frequency of transmitted signals and the sinusoidal frequency generated by an oscillator of a mixer. The frequency offset F_{os} produces a phase shift of $2\pi F_{os}t$ in the baseband signals.

2.2.1 Maximum-Likelihood Estimation (MLE) of a Single RF Impairment

We will present the signal models when a single RF impairment - either nonlinearity or frequency offset - is present, as well as introduce the maximum-likelihood estimation (MLE) in the previous studies.

Baseband Signal Model for Estimation of Nonlinearity

The nonlinear behavior of the RF circuit is represented by the third order gain α_3 in a cubic function as below,

$$v_{out}(t) = \alpha_1 v_{in}(t) + \alpha_2 v_{in}(t)^2 + \alpha_3 v_{in}(t)^3. \tag{2.15}$$

The input signal $v_{in}(t)$ is the transmitted pass-band signal $x^p(t)$ of carrier frequency ω_c,

$$x^p(t) = x^I(t)\sqrt{2}\cos\omega_c t + x^Q(t)\sqrt{2}\sin\omega_c t. \tag{2.16}$$

where $x^I(t)$ and $x^Q(t)$ are in-phase and quadrant base-band signals.

We first analyze signal models and build the equivalent base-band models of impairment parameters. We assume that the transmitted base-band signal is $x(t) = x^I(t) + j \cdot x^Q(t)$, the baseband signal $z(t)$ is received from the RF front-end receiver system, and there is no interference signal in our signal model. The base-band signal $z(t)$ is expressed in terms of the first order gain α_1, the third order (nonlinearity) gain α_3, as well as thermal noise $n(t)$ given as below,

$$z(t) = \alpha_1 x(t) + 3\alpha_3 x(t)|x(t)|^2 + n(t), \tag{2.17}$$

where α_1 and α_3 are the overall gains by all amplifiers and mixers in the RF front-end and $n(t) = \alpha_1 n_0(t)$ and $n_0(t)$ is thermal noise at the antenna.

Notice that the second order gain α_2 does not affect the base-band signal $z(t)$, and thus, can be ignored. A vector $\mathbf{Z_T}$ is composed of the samples of $z(t)$ with sampling time T_s.

$$\mathbf{Z_T} = [z(T_s), z(2T_s), \cdots, z(nT_s), \cdots, z(NT_s)]^T. \tag{2.18}$$

Also, a vector $\mathbf{X_T}$ and a vector $\mathbf{V_T}$ are obtained from the samples of $x(t)$ and $v(t)$ where $v(t) = 3x(t)|x(t)|^2$.

$$\begin{aligned} \mathbf{X_T} &= [x(T_s), x(2T_s), \cdots, x(nT_s), \cdots, x(NT_s)]^T, \\ \mathbf{V_T} &= [v(T_s), v(2T_s), \cdots, v(nT_s), \cdots, v(NT_s)]^T. \end{aligned} \tag{2.19}$$

The relationship of vectors in (2.18) and (2.19) is

$$\mathbf{Z_T} = \alpha_1 \mathbf{X_T} + \alpha_3 \mathbf{V_T} + \mathbf{N_T}. \tag{2.20}$$

The vector $\mathbf{N_T}$ consists of samples of noise $n(t)$ having a normal distribution with mean zero.

The least-square estimators of parameters α_1 and α_3 are obtained by minimizing the power of the noise term $\mathbf{N_T}$ in (2.20) as follows,

$$[\widehat{\alpha_1} \quad \widehat{\alpha_3}] = \underset{\alpha_1,\alpha_3}{\operatorname{argmin}} ||\mathbf{Z_T} - (\alpha_1 \mathbf{X_T} + \alpha_3 \mathbf{V_T})||^2. \tag{2.21}$$

Then, maximum-likelihood estimators (MLE) $\widehat{\alpha_1}$ and $\widehat{\alpha_3}$ are given as,

$$[\widehat{\alpha_1} \quad \widehat{\alpha_3}]^T = (\mathbf{\Psi}^H \mathbf{\Psi})^{-1} \mathbf{\Psi}^H \mathbf{Z_T}, \tag{2.22}$$

where the basis matrix $\mathbf{\Psi}$ is defined as $\mathbf{\Psi} = [\mathbf{X_T} \quad \mathbf{V_T}]$ [1].

Baseband Signal Model for Estimation of Frequency Offset

The frequency offset represents the mismatch of the carrier frequency of transmitted signals and the sinusoidal frequency generated by an oscillator of a mixer. The frequency offset F_{os} produces a time-varying phase shift defined by $2\pi F_{os} t$ in the baseband signals.

The received baseband signal $z(t)$ contains the first order gain α_1, frequency offset F_{os} with noise $n(t)$ of a Gaussian distribution,

$$z(t) = \alpha_1 x(t) e^{j2\pi F_{os} t} + n(t). \tag{2.23}$$

The normalized frequency offset ξ is defined as,

$$\xi = \frac{F_{os}}{F_s/N}, \tag{2.24}$$

where F_s is the sampling frequency and N is the number of symbols in OFDM [12].

The normalized frequency offset ξ is estimated as [12],

$$\widehat{\xi} = \frac{1}{2\pi} arg \left(\sum_{n=1}^{N} (\mathbf{Z_T})_n^* (\mathbf{Z_T})_{n+N} \right), \tag{2.25}$$

where $(\mathbf{Z_T})_n$ is the n-th element of the vector $\mathbf{Z_T}$.

2.2.2 Joint Estimation of RF Impairments

Now, we will consider joint RF impairments -nonlinearity and frequency offset- in a baseband signal model and design invariant estimators for gain, nonlinearity, frequency offset and noise figure.

Baseband Signal Model for Joint Estimation of Nonlinearity and Frequency Offset

The received baseband signal $z(t)$ contains the first order gain α_1, the third order gain α_3, frequency offset F_{os}, as well as thermal noise $n(t)$ as below,

$$z(t) = \alpha_1 x(t) e^{j2\pi F_{os} t} + 3\alpha_3 x(t)|x(t)|^2 e^{j2\pi F_{os} t} + n(t). \tag{2.26}$$

The relationship of the vectors $\mathbf{Z_T}$, $\mathbf{X_T}$, $\mathbf{V_T}$ and $\mathbf{H_T}$ is given as below,

$$\mathbf{Z_T} = \mathbf{H_T}(\alpha_1 \mathbf{X_T} + \alpha_3 \mathbf{V_T}) + \mathbf{N_T}, \tag{2.27}$$

where $\mathbf{Z_T}$, $\mathbf{X_T}$, $\mathbf{V_T}$ are given in (2.18) and (2.19), and the diagonal matrix $\mathbf{H_T}$ has the n-th diagonal element of $e^{j2\pi F_{os} n T_s}$. The vector $\mathbf{N_T}$ consists of samples of noise $n(t)$.

The vector $\mathbf{Z_T}$ of a discrete-*time* signal is transformed to the vector $\mathbf{Z_F}$ of a discrete-*frequency* signal using the *Discrete Fourier Transform* (DFT). In order to calculate the DFT of $\mathbf{H_T X_T}$ and $\mathbf{H_T V_T}$ in (2.27), the following three properties of the Fourier Transform are useful.

(A) DFT is not only calculated directly from a discrete-time signal, but it can also be obtained by sampling the *Discrete Time Fourier Transform* (DTFT) of the time signal.

(B) In DTFT, multiplication of the diagonal matrix $\mathbf{H_T}$ (composed of the n-th diagonal element of $e^{j2\pi F_{os} n T_s}$) in the time domain is equivalent to the frequency shift by $F_{os} T_s$ in the frequency domain.

(C) DTFT can be reconstructed from DFT -inverse to property (A)- when DFT is convo-

luted with the phase-shifted Dirichlet function $P_N(f)$:

$$\begin{aligned} P_N(f) &= \frac{sin(\pi f N)}{sin(\pi f)} e^{-j\pi f(N-1)} \\ &\approx sinc(Nf) e^{-j\pi f(N-1)}. \end{aligned} \tag{2.28}$$

(the above approximation is valid when N is large enough.)

From property (C), the DTFT $X(f)$ of the time signal $x[n] = (\mathbf{X_T})_n$ is,

$$X(f) = \frac{1}{N} \sum_{n=0}^{N-1} (\mathbf{X_F})_n P_N \left(f - \frac{n}{N} \right), \tag{2.29}$$

where the vector $\mathbf{X_F}$ is obtained from the DFT of $(\mathbf{X_T})_n$.

Because the signal $X(f)$ is the DTFT of $(\mathbf{X_T})_n$, property (B) proves that the signal $X(f - \xi/N)$ is the DTFT of $\mathbf{H_T X_T}$.

By property (A), the sampled signal of $X(f - \xi/N)$ at every $f = \frac{k}{N}$, where $k \in \{0, 1, \cdots, N-1\}$, is the same as the DFT of $\mathbf{H_T X_T}$. In the same manner, the DFT of $\mathbf{H_T V_T}$ is obtained.

Therefore, the DFT $(\mathbf{Z_F})_k$ of the discrete signal $(\mathbf{Z_T})_n$ in (2.27) is expressed as,

$$\begin{aligned} (\mathbf{Z_F})_k &= \alpha_1 \sum_{n=0}^{N-1} (\mathbf{X_F})_n \cdot P_N \left(\frac{k - n - \xi}{N} \right) \\ &+ \alpha_3 \sum_{n=0}^{N-1} (\mathbf{V_F})_n \cdot P_N \left(\frac{k - n - \xi}{N} \right). \end{aligned} \tag{2.30}$$

When the function $P_N(\cdot)$ is approximated, $(\mathbf{Z_F})_k$ is approximated to,

$$\begin{aligned} (\mathbf{Z_F})_k &\cong \alpha_1 (\mathbf{X_F})_n \cdot sinc\,(0 - \xi)\, e^{j\pi\xi \frac{N-1}{N}} \\ &+ \alpha_3 (\mathbf{V_F})_n \cdot sinc\,(0 - \xi)\, e^{j\pi\xi \frac{N-1}{N}}. \end{aligned} \tag{2.31}$$

Also, the functions $sinc(\cdot)$ and $exp(\cdot)$ are approximated by Taylor series: $sinc(x) \approx 1 - \frac{1}{6}x^2$ and $e^x \approx 1 + x$ when x is small enough, and $sinc(\cdot)$ is an even function. The

function $sinc(\cdot)exp(\cdot)$ is approximated to $1+kx$, which is substituted into (2.31). A new vector equation is derived as follows,

$$\mathbf{Z_F} = \alpha_1(\mathbf{X_F} + \xi\mathbf{U_F}) + \alpha_3(\mathbf{V_F} + \xi\mathbf{W_F}) + \mathbf{N_F}. \tag{2.32}$$

Practically, the vector $\mathbf{W_F}$ is small enough to discard. Therefore, we derive the final subspace model of baseband signals with joint RF impairments:

$$\mathbf{Z_F} = \alpha_1\mathbf{X_F} + \alpha_1\xi\mathbf{U_F} + \alpha_3\mathbf{V_F} + \mathbf{N_F}. \tag{2.33}$$

Invariance and Joint Estimation

Based on (2.33), we can design the estimators of α_1, α_3, F_{os} in a reconfigurable RF front-end. While the original baseband signal model (2.26) shows the effect of multiple RF impairments, the linearization resulting (2.33) allows us to design (nearly) invariant

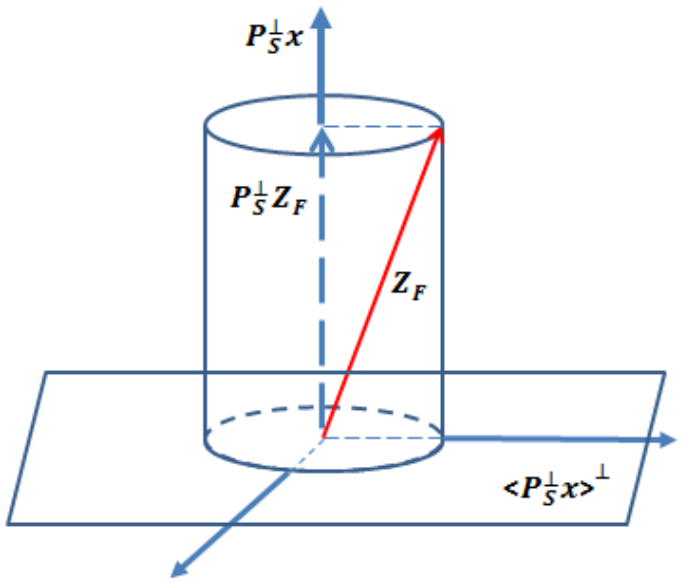

Figure 2.9: The projection matrix $\mathbf{P_S^{\perp}}$ projects the received signal $\mathbf{Z_F}$ to the orthogonal complement of the column subspace of $\mathbf{S}$: $\mathbf{P_S^{\perp}Z_F}$

estimators for these parameters. In [7], we show this for all the above parameters. But for the present purpose, we only describe how to estimate the frequency offset F_{os}.

The idea of our invariant estimators is that the received signal $\mathbf{Z_F}$ is projected onto the orthogonal complement of the basis vectors corresponding to nuisance parameters. We need to design the projection matrix for the transformation of basis vectors and the vector $\mathbf{Z_F}$ of a received signal into the new orthogonal subspace (Figure 2.9).

To describe the invariant estimator, suppose the distribution of the vector $\mathbf{Z_F}$ is given as $N(\mu\mathbf{x} + \mathbf{S}\phi, \sigma^2\mathbf{I})$ where the parameters μ, ϕ and σ are unknown and the vector $\mathbf{x}$, the column matrix $\mathbf{S}$ are known and $\mathbf{I}$ is an identity matrix. In order to estimate the parameter μ invariant to nuisance parameter ϕ, we eliminate the matrix $\mathbf{S}$ in the mean $\mu\mathbf{x} + \mathbf{S}\phi$. Assume that a projection matrix $\mathbf{P}_{\mathbf{S}}^{\perp}$ projects a vector to the orthogonal complement of the column space of the matrix $\mathbf{S}$. The vector $\mathbf{P}_{\mathbf{S}}^{\perp}\mathbf{Z_F}$ has distribution $N(\mu\mathbf{x}', \sigma'^2 I)$ where $\mathbf{x}' = \mathbf{P}_{\mathbf{S}}^{\perp}\mathbf{x}$ and σ' is a variance of noise in the projected subspace. Then, the invariant estimator $\widehat{\mu}$ is designed as follows,

$$\widehat{\mu} = \mathbf{x}'^T\mathbf{P}_{\mathbf{S}}^{\perp}\mathbf{Z_F}/(\mathbf{x}'^T\mathbf{x}'). \tag{2.34}$$

('Invariance' refers to the fact that the distribution of the estimate $\widehat{\mu}$ is unaffected by the nuisance parameter ϕ in [15, 16].)

Gain The estimator of $\widehat{\alpha_1}$ is obtained by defining parameters in (2.34) as follow:

$$\mu = \alpha_1, \qquad \mathbf{x} = \mathbf{X_F}$$
$$\mathbf{S} = [\mathbf{U_F} \quad \mathbf{V_F}], \quad \phi = [\alpha_1\xi \quad \alpha_3]^T,$$

where the vectors $\mathbf{X_F}$, $\mathbf{U_F}$, $\mathbf{V_F}$ are the basis vectors in (2.33).

Defining a vector $\mathbf{x}' = \mathbf{P}_{\mathbf{S}}^{\perp} \cdot \mathbf{x} = \mathbf{P}_{\mathbf{S}}^{\perp} \cdot \mathbf{X}_{\mathbf{F}}$, the designed estimator $\widehat{\alpha_1}$ is obtained as,

$$\widehat{\alpha_1} = \mathbf{x}'^T \mathbf{P}_{\mathbf{S}}^{\perp} \mathbf{Z}_{\mathbf{F}} / (\mathbf{x}'^T \mathbf{x}'). \tag{2.35}$$

Nonlinear Parameter, IP3 The estimator $\widehat{\alpha_3}$ is obtained by defining parameters in (2.34) as,

$$\mu = \alpha_3, \qquad \mathbf{x} = \mathbf{V}_{\mathbf{F}}$$
$$\mathbf{S} = [\mathbf{X}_{\mathbf{F}} \quad \mathbf{U}_{\mathbf{F}}], \quad \phi = [\alpha_1 \quad \alpha_1 \xi]^T.$$

We can estimate for obtaining $\widehat{\alpha_3}$ in (2.34) and using Algorithm 3.

Then, we converted $\widehat{\alpha_3}$ to a third-order intercept point (IP3), a standardized parameter representing for nonlinearity of RF systems.

$$\widehat{\text{IP3}} = \frac{\widehat{\alpha_1}}{\widehat{\alpha_3}} \cdot \frac{4}{3}. \tag{2.36}$$

Frequency Offset The estimator $\widehat{\xi}$ of normalized frequency offset is calculated by defining,

$$\mu = \alpha_1 \xi, \qquad \mathbf{x} = \mathbf{U}_{\mathbf{F}}$$
$$\mathbf{S} = [\mathbf{X}_{\mathbf{F}} \quad \mathbf{V}_{\mathbf{F}}], \quad \phi = [\alpha_1 \quad \alpha_3]^T.$$

After calculating $\widehat{\mu}$ in (2.34), the estimator $\widehat{\xi}$ is given as,

$$\widehat{\xi} = \widehat{\mu} / \widehat{\alpha_1}. \tag{2.37}$$

Based on the idea of invariant estimation presented in (2.34), we designed the estimators of ξ (which is the normalized frequency offset), where the projection matrix $\mathbf{P}_{\mathbf{S}}^{\perp}$ is obtained by Algorithm 3.

After calculating $\widehat{\mu}$ in (2.34), the estimator $\widehat{\xi}$ is given as,

$$\widehat{\xi} = \widehat{\mu} / \widehat{\alpha_1}. \tag{2.38}$$

Algorithm 3 find the matrix $\mathbf{P}_{\mathbf{S}}^{\perp}$, which projects a vector to the orthogonal complement of column space of $\mathbf{S}$.

$K \leftarrow$ the number of columns in the matrix $\mathbf{S}$.
$\mathbf{Q} \leftarrow \mathbf{I}$.
for $k = 1, 2, \cdots, K$ **do**
    $\mathbf{y} \leftarrow$ the k-th column vector of the matrix $\mathbf{S}$.
    $\mathbf{y_1} \leftarrow \mathbf{Q}^T \cdot \mathbf{y}$.
    $\mathbf{P_y} = \mathbf{y_1}\mathbf{y_1}^T/(\mathbf{y_1}^T\mathbf{y_1})$.
    $\mathbf{P_y}^{\perp} = \mathbf{I} - \mathbf{P_y}$.
    $\mathbf{Q} \leftarrow \mathbf{Q} \cdot \mathbf{Q_k}$.
end for
$\mathbf{P}_{\mathbf{S}}^{\perp} \leftarrow \mathbf{Q}^T$.

The estimator $\widehat{\alpha_1}$ of the k-th configuration is calculated from $\widehat{G_k}$ in (2.4) estimated in Factory mode, using the following formula,

$$\widehat{\alpha_1} = 10^{\widehat{G_k}/20}. \tag{2.39}$$

Estimate of Noise Figure In (2.33), the signal model $\mathbf{Z_F}$ is defined by the multivariate normal distribution $N(\mathbf{S}\phi, \sigma_n^2\mathbf{I})$ where $\mathbf{S} = [\mathbf{X_F} \quad \mathbf{U_F} \quad \mathbf{V_F}]$, $\phi = [\alpha_1 \quad \alpha_1\xi \quad \alpha_3]^T$, and $\sigma_n^2 = \alpha_1^2\sigma^2$. The projection matrix $\mathbf{P}_{\mathbf{S}}^{\perp}$ has one more vector and is calculated using Algorithm 3. Then,

$$\widehat{\sigma^2} = Var(\mathbf{P}_{\mathbf{S}}^{\perp}\mathbf{Z_F})/\alpha_1^2, \tag{2.40}$$

where $Var(\cdot)$ denotes sample variance.

The estimated noise figure $\widehat{NF}$ is defined as $\widehat{NF} = 10 \cdot \log_{10}\left(\widehat{\sigma^2}/(kTB)\right)$, where k is the Boltzmann constant, T is the current temperature in Kelvin, and B is bandwidth of the IF filter before sampling.

Gain after Bias Compensation We have assumed that $v_{in}(t) = x(t)$ in (2.15) and noise $n(t) = \alpha_1 n_0(t)$, where $n_0(t)$ is antenna noise, an additive white Gaussian noise (AWGN).

However, the input signal $v_{in}(t)$ is equal to $x(t) + n_0(t)$, and thus, the noise term $n(t)$ is complicated as follows,

$$n(t) = \alpha_1 n_0(t) + \alpha_3 n_0(t)^* x(t)^2 + 2\alpha_3 n_0(t)|x(t)|^2$$
$$+2\alpha_3|n_0(t)|^2 x(t) + \alpha_3 n_0(t)^2 x(t)^* + \alpha_3|n_0(t)|^2 n_0(t)), \tag{2.41}$$

where it is assumed that $E[n_0(t)] = 0$, $E[x^*(t)] = 0$, $E[|n_0(t)|^2] = \sigma^2$, $|n_0(t)|^2 n_0(t))$ is small enough to be ignored. Then, after averaging the noise $n(t)$, the fourth term $2\alpha_3|n_0(t)|^2 x(t)$ is placed in the subspace of $\mathbf{X_F}$ causing bias on the estimator of α_1 while other terms are ignored as noise. The bias-compensated estimator $\widehat{\alpha_1}'$ is given as,

$$\widehat{\alpha_1}' = \widehat{\alpha_1} - 2 \cdot \widehat{\alpha_3} \cdot \widehat{\sigma^2}. \tag{2.42}$$

Calibration of Basis Vectors

The basis vectors $\mathbf{X_F}$, $\mathbf{U_F}$ and $\mathbf{V_F}$ of the linear model in (2.33) are obtained from the calibration of simulation. For example, for obtaining the basis of gain, two signals pass through the RF front-end for two different values of gain while other RF impairments are fixed. The difference of the two obtained signals is normalized by the gain difference in order to obtain the basis vector $\mathbf{X_F}$. Other basis vectors are obtained similarly.

2.2.3 Simulation and Results

Simulation Setup

In order to validate the RF impairment estimators designed in Section 2.2.2, we implemented and simulated a reconfigurable RF front-end in MATLAB Simulink as shown in Figure 2.3 and 2.4. There are 1080 configurations of a reconfigure RF front-end by

Table 2.2: Simulation Setup

Channel Property	AWGN channel
Pulse-shaping filter p(t)	Square-root raised cosine filter Roll-off factor 0.2
Communication Standard	802.11a (OFDM system) OFDM symbol size N=64
Carrier Frequency	2.4 GHz (WLAN environment)
Symbol Rate	20 MHz
Frequencies in RF system	3.6 GHz, 6.0 GHz
Signal Constellation	BPSK
Received Signal Power	-75 dBm
Gain (α_1)	0 dB to 20 dB increased by 4 dB
Nonlinearity (IP3)	0 to -40 dBm decreased by -10 dBm
Frequency Offset (F_{os})	0 to 50 kHz increased by 10 kHz
Noise Figure (NF)	0 dB to 25 dB increased by 5 dB
Signal-to-Noise Ratio (SNR)	0 to 25 dB increased by 5 dB

tuning gain and IP3 of amplifiers, frequency offset in mixers, and noise figure. In the simulation, we collected baseband signals received after passing though the RF front-end of the configuration. The baseband signals for each configuration are used for estimating RF impairments of the configuration. The IEEE 802.11a standard is set as a baseband communication system. The details of the setup parameters are specified in Table 2.2.

Simulation Results

Simulation results of RF impairment estimation are observed for our invariant estimators presented in Section 2.2.2 as well as the MLE estimators in Section 2.2.1. Varying SNR from 0 to 25 dB, the normalized mean square errors (NMSE) of gain, IP3 and noise figure are given in Figures 2.10, 2.11 and 2.13, respectively, and mean square error (MSE) of normalized frequency offset is given in Figure 2.12.

The NMSE of invariant estimates of gain in (2.35) drops as SNR increases and the NMSE of the MLE estimates in (2.22) does so in Figure 2.10. However, the MLE estimates (black) have higher gain estimation error than invariant estimates (blue). This is because our invariant estimator is invariant to other nuisance impairments such as frequency offset while the MLE estimator of gain is not. Still, the invariant estimates are slightly biased by interaction noise and nonlinearity. However, the bias-compensated estimator in (2.42) (red) additionally improved the accuracy of the gain estimator.

The NMSE's of IP3 estimator are plotted against SNR for three received signal powers of -75 dBm, -43 dBm and -29 dBm, respectively, as seen in Figure 2.11. The NMSE of our invariant estimators in (2.36) improves its accuracy when signal power is increased from -75 dBm to -43 dBm and -29 dBm (blue, yellow, red, respectively). This is because the power of the cubed signal $x(t)|x(t)|^2$ is significantly small enough to be buried under noise power. Thus, increased signal power distinguishes the basis vector of nonlinear components and improves the accuracy of IP3 estimator. Meanwhile, the MLE estimator of IP3 using (2.22) suffers from frequency offset as well as gain, even with increased signal powers (pink). When IP3 is higher (i.e., more linear), the influence of gain estimation error causes a significant bias in the MLE estimator of IP3.

The MSE's of normalized frequency offset are plotted against SNR in Figure 2.12. The MLE estimator of frequency offset in (2.25) is also invariant to gain and IP3 just like

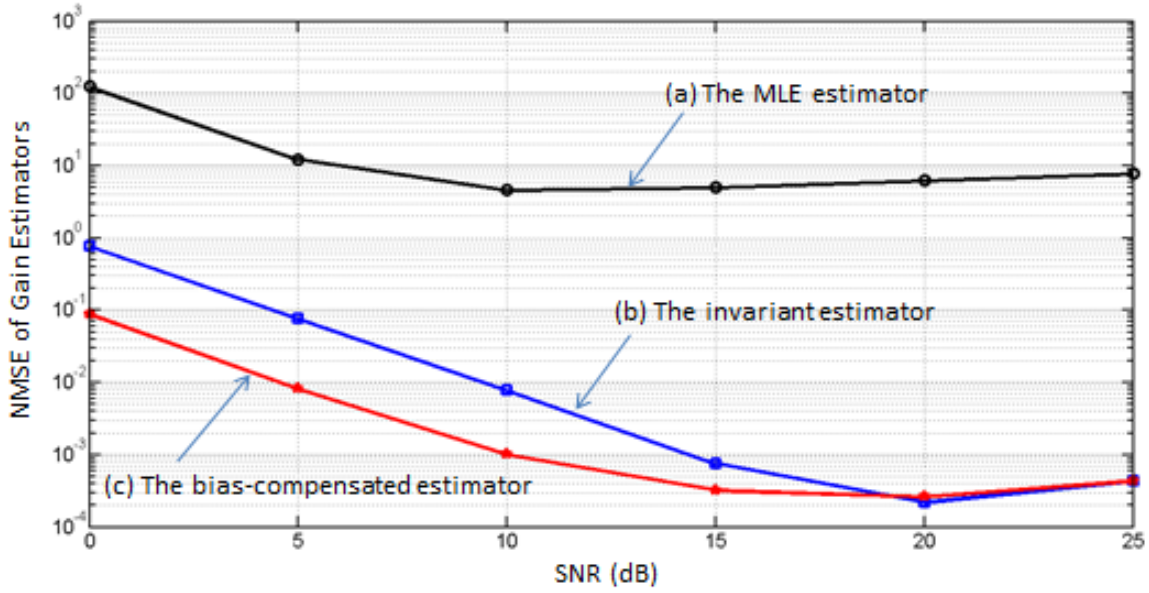

Figure 2.10: the NMSE of gain against SNR: (a) the MLE estimator of gain in (2.22) (black); (b) the invariant estimator of gain in (2.35) (blue) ; (c) the bias-compensated estimator of gain in (2.42) (red).

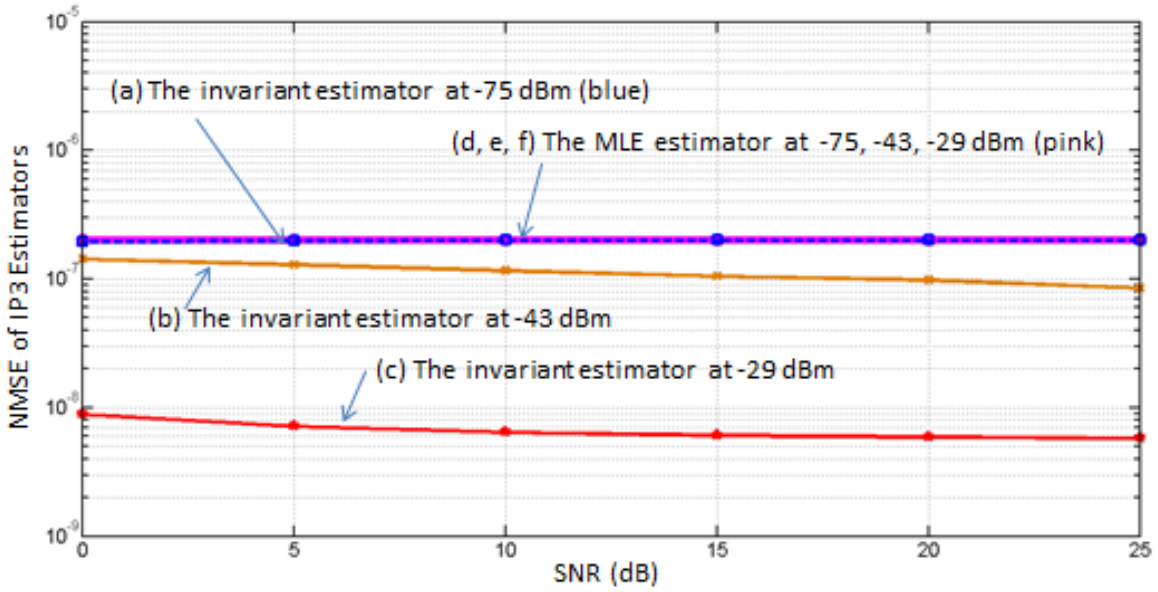

Figure 2.11: the NMSE of IP3 against SNR: the invariant estimator of IP3 in (2.36) at received signal power of (a) -75 dBm (blue), (b) -43 dBm (yellow), (c) -29 dBm (red), respectively; the MLE estimates of IP3 in (2.22) at received signal power of (d) -75 dBm, (e) -43 dBm, (f) -29 dBm (all in pink).

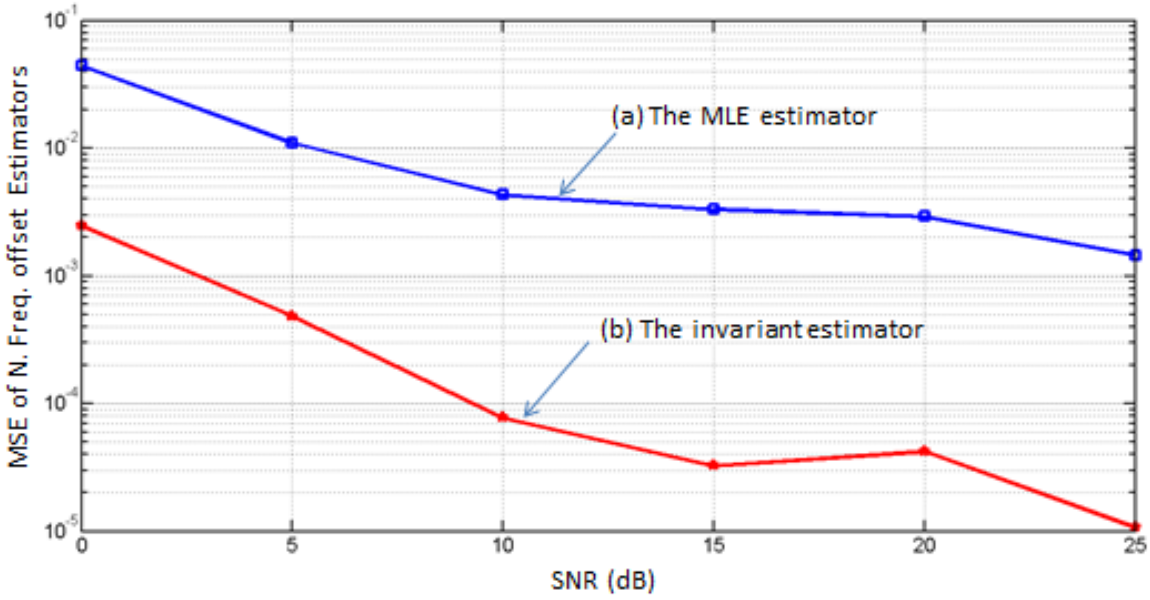

Figure 2.12: the MSE of normalized frequency offset against SNR: (a) the MLE estimator in (2.25) (blue); (b) the invariant estimator in (2.37) (red).

our invariant estimator in (2.37). However, the MSE of the MLE estimates is higher than that of the invariant estimates of frequency offset. The normalized frequency offset ξ is ranged from 0 to 0.2 in order to validate the linear approximation in (2.32).

The NMSE's of NF estimates in Equation 2.40 are plotted against SNR in Figure 2.13 for four cases: all possible configurations (black); configurations for fixed IP3 of 0 dBm (red); configurations for fixed frequency offset of 0 Hz (blue); configurations with fixed IP3 of 0 dBm and frequency offset of 0 Hz (green). We found that when noise figure (i.e., noise power) is higher, the NMSE's are higher. The NMSE's of the noise figure without frequency offset (black and red) are more accurate than that with frequency offset (blue and green). This is because the basis vector of frequency offset are approximated using Taylor series expansion, and additional nonlinear polynomial terms are included within the measurement of noise.

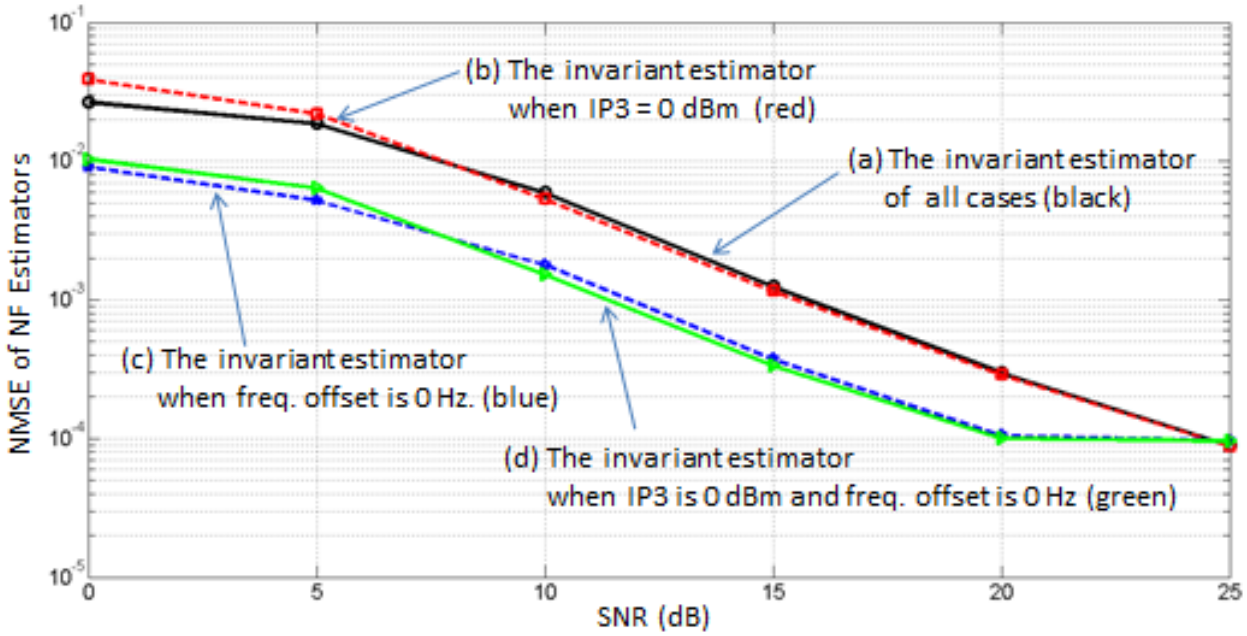

Figure 2.13: the NMSE of noise figure against SNR: the invariant estimators in (2.40) of (a) all cases (black); (b) when IP3 is given as 0 dBm (red); (c) when frequency offset is given as 0 Hz (blue); (d) when IP3 is 0 dBm and frequency offset is 0 Hz (green).

In this chapter, we have studied estimation method of gain, nonlinearity, phase noise, noise figure and frequency offset. The estimated RF impairments are useful for predicting the communication quality represented by the metric SINR, as discussed in the next chapter.

Chapter 3

Environment Adaptable Fast (EAF) Optimization

In order to hasten an optimization process, in this chapter, we first obtain a useful metric, the calculated Signal-to-Interference-and-Noise Ratio (SINR). The calculated SINR allows us to predict the communication quality of each configuration. Based on this calculated SINR, we are able to prune out the configurations that are not likely to meet the requirement of a given communication standard, thus allowing EAF optimization in In-theater mode (Appendix B).

3.1 SINR Calculation

In this section, we derive the formula for calculating SINR based on the estimated RF impairments. The SINR of the k-th configuration is calculated in terms of phase noise, nonlinearity and noise figure.

$$\text{SINR}^{(k)} = \frac{P_S}{{P_{phn}}^{(k)} + {P_{ip3}}^{(k)} + {P_n}^{(k)}}, \tag{3.1}$$

where P_S is the signal power. ${P_{phn}}^{(k)}$ is the impairing signal power by phase noise impairment, ${P_{ip3}}^{(k)}$ is the impairing signal power by third order nonlinearity impairment, and ${P_n}^{(k)}$ is the impairing signal power by thermal noise impairment.

3.1.1 Phase Noise Impairment

The impairing signal power ${P_{phn}}^{(k)}$ is given as,

$$ {P_{phn}}^{(k)} = {P_{phn,S}}^{(k)} + {P_{phn,I}}^{(k)}, \tag{3.2} $$

where ${P_{phn,S}}^{(k)}$ is due to the signal of interest, and ${P_{phn,I}}^{(k)}$ is due to interferers.

Phase Noise and the Signal of Interest

The first term ${P_{phn,S}}^{(k)}$ is calculated by the following equation,

$$ {P_{phn,S}}^{(k)}{}_{(dBm)} = P_{S(dBm)} + \int_{-\inf}^{\inf} L^{(k)}(f)df \Big|_{(dB)}, \tag{3.3} $$

where $L^{(k)}(f)$ is the phase noise spectral density of the k-th configuration at the offset frequency f. Phase noise spectral density is estimated in Factory mode as shown in Section 2.1.2.

Phase Noise and Interference

The impairing signal power ${P_{phn,I}}^{(k)}$ is,

$$ {P_{phn,I}}^{(k)} = \sum_j {P_{phn,I_j}}^{(k)}, \tag{3.4} $$

where the interferer I_j has the power P_{I_j}. When I_j is located at the offset frequency f_j, ${P_{phn,I_j}}^{(k)}$ is,

$$ {P_{phn,I_j}}^{(k)}{}_{(dBm)} = P_{I_j\,(dBm)} + L^{(k)}(f_j)_{(dBc/Hz)} + B_{(dB)}, \tag{3.5} $$

where B is the bandwidth of the signal of interest.

The phase noise spectral density $L^{(k)}(f)$ is assumed to be calculated in Factory mode using the estimation method presented in Section 2.1.2.

3.1.2 Third Order Nonlinearity Impairment

We will calculate ${P_{ip3}}^{(k)}$ as follows,

$$ {P_{ip3}}^{(k)} = {P_{ip3,S}}^{(k)} + {P_{ip3,S,I}}^{(k)} + {P_{ip3,I}}^{(k)}. \tag{3.6} $$

where ${P_{ip3,S}}^{(k)}$ is the impairing signal power due to the signal of interest, ${P_{ip3,S,I}}^{(k)}$ is the impairing signal power due to intermodulation of the signal of interest and interference, and ${P_{ip3,I}}^{(k)}$ is the impairing signal power due to interference.

Nonlinearity and the Signal of Interest

If there is no interference, the impairing signal power ${P_{ip3,S}}^{(k)}$ is given as,

$$ {{P_{ip3,S}}^{(k)}}_{(dBm)} = 3 \cdot P_{S(dBm)} - 2 \cdot {\text{IIP}_3}^{(k)}{}_{(dBm)}, \tag{3.7} $$

where ${\text{IIP}_3}^{(k)}$ is the Input Third-order Intercept Point (IIP3) of the k-th configuration. ${\text{IIP}_3}^{(k)}$ is assumed to be estimated in Factory mode using the estimation method presented in Section 2.1.1

Nonlinearity and the Signal of Interest and Interference

If there is any interference within the passband of IF filter, the signal of interest and the interferer are intermodulated as follows,

$$ \begin{aligned} y^p(t) &= \alpha_1(x^p(t) + Acos(2\pi(f_c + f_0)t)) \\ &\quad +\alpha_3(x^p(t) + Acos(2\pi(f_c + f_0)t))^3. \end{aligned} \tag{3.8} $$

Then, (3.8) is expanded to,

$$\begin{aligned} y^p(t) &= \alpha_1 x^p(t) + \alpha_1 A cos(2\pi(f_c + f_0)t) \\ &\quad + \alpha_3 x^p(t)^3 + 3\alpha_3 x^p(t)^2 A cos(2\pi(f_c + f_0)t) \\ &\quad + 3\alpha_3 x^p(t) A^2 cos^2(2\pi(f_c + f_0)t) \\ &\quad + \alpha_3 A^3 cos^3(2\pi(f_c + f_0)t), \end{aligned} \tag{3.9}$$

where $x^p(t) = x^I(t)cos(2\pi f_c t) + x^Q(t)sin(2\pi f_c t)$.

In (3.9), the second, the fourth and the sixth terms are filtered out because these terms are out of band. The first term is the signal of interest, and the third term was already considered in (3.7). The fifth term is rewritten as,

$$\frac{3}{2}\alpha_3 x^p(t) A^2 \left(1 + cos(4\pi(f_c + f_0)t)\right). \tag{3.10}$$

While the second term at $2(f_c + f_0)$ Hz is filtered out, the first term at f_c still interferes with the signal of interest at f_c.

Then, the intermodulated signal by the signal of interest and interference is given as,

$$P_{ip3,S,I}{}^{(k)} = \sum_j P_{ip3,S,Ij}{}^{(k)}, \tag{3.11}$$

$$P_{ip3,S,Ij}{}^{(k)}{}_{(dBm)} = P_{S(dBm)} + 2 \cdot P_{Ij_{(dBm)}} - 2 \cdot \text{IIP}_3{}^{(k)}{}_{(dBm)}.$$

Nonlinearity and Interference

Finally, impairing signals I_j are caused by intermodulation of two interferers at the frequency $f_{Ij,1}$ and $f_{Ij,2}$, respectively, when the two interferers satisfy the condition $2 \cdot f_{Ij,1} = f_{Ij,2} + f_c$. The impairing signal power resulting from the intermodulation of the interference is given as,

$$P_{ip3,I}{}^{(k)} = \sum_j P_{ip3,Ij}{}^{(k)}, \tag{3.12}$$

$$P_{ip3,Ij}{}^{(k)}{}_{(dBm)} = 2 \cdot P_{Ij,1(dBm)} + P_{Ij,2(dBm)} - 2 \cdot \text{IIP}_3{}^{(k)}{}_{(dBm)},$$

where two interferers of the power $P_{Ij,1}$ and $P_{Ij,2}$ respectively are intermodulated.

3.1.3 Noise Figure Impairment

Finally, $P_n{}^{(k)}$ is obtained from the noise figure impairment obtained in Section 2.1.3.

$$P_n{}^{(k)}{}_{(dB)} = \widehat{NF}{}^{(k)}_{(dB)} + (kTB)_{(dB)}, \tag{3.13}$$

where $\widehat{NF}{}^{(k)}$ is the estimated noise figure of the k-th configuration, k is the Boltzmann constant, T is the current temperature in Kelvin, and B is the bandwidth of the IF filter before sampling.

3.1.4 Simulation

Simulation Setup

We verified the performance of calculated SINR in (3.1) using Matlab Simulink in Figure 2.3 and 2.4. In the simulation, the standard IEEE 802.11g is used. The transmitted signal of -67 dBm has the bandwidth 20 MHz, and a strong narrowband blocker of -35 dBm at an offset frequency of 20 MHz. We simulated 216 sample configurations and compared their simulated SINR with calculated SINR.

Simulation Results

In Figure 3.1, we plotted simulated SINR on the y-axis and calculated SINR on the x-axis. We colored the data point for the k-th configuration according to the type of a dominant impairing signal power: $P_{phn,I}{}^{(k)}$ in (3.4) (pink), $P_{ip3,I}{}^{(k)}$ in (3.12) (blue), $P_n{}^{(k)}{}_{(dB)}$ in

(3.13) (black). The simulation results demonstrate the accuracy of the calculated SINR in (3.1).

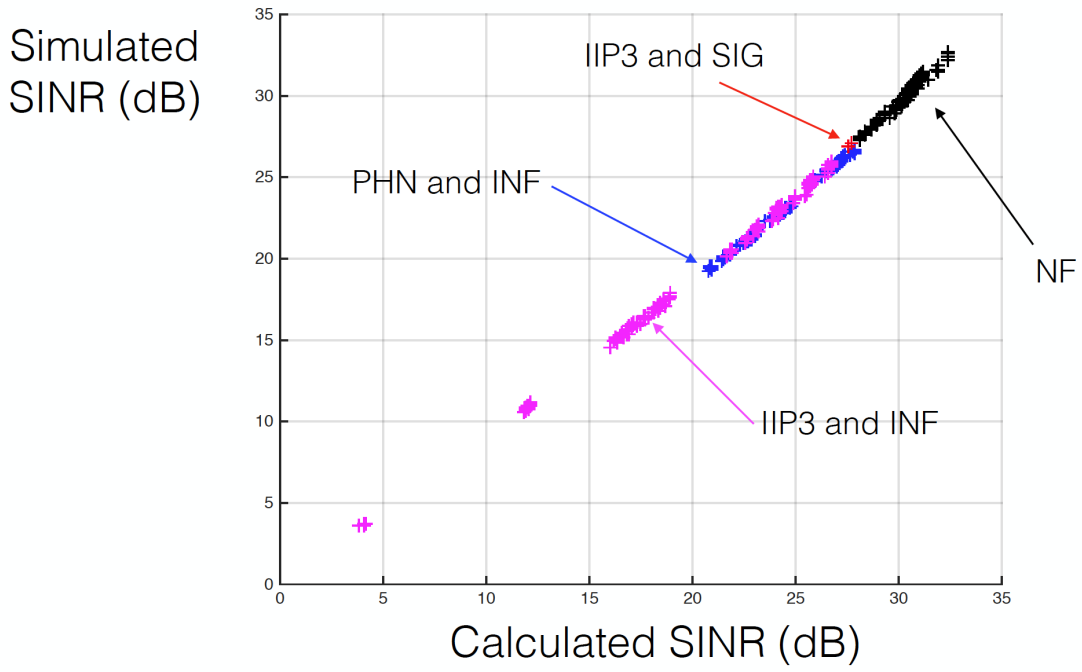

Figure 3.1: Simulation Results - calculated SINR in (3.1) is on the x-axis and simulated SINR is on the y-axis. The data point for the k-th configuration is colored according to the type of a dominant impairing signal power: ${P_{phn,I}}^{(k)}$ in (3.4) (pink), ${P_{ip3,I}}^{(k)}$ in (3.12) (blue), ${P_n}^{(k)}{}_{(dB)}$ in (3.13) (black).

The signal spectrum required for calculating SINR can be obtained by a *Spectrum Analyzer*. The Spectrum Analyzer obtains the power of both blockers and the signal of interest, and center frequencies while we did not explicitly consider the design of a Spectrum Analyzer, we note that this can be easily implemented if the reconfigurable radio uses a homodyne architecture in Figure 3.2. The Spectrum Analyzer operates by observing received signals in frequency domain while tuning the sinusoidal frequency of a local oscillator in a mixer [5].

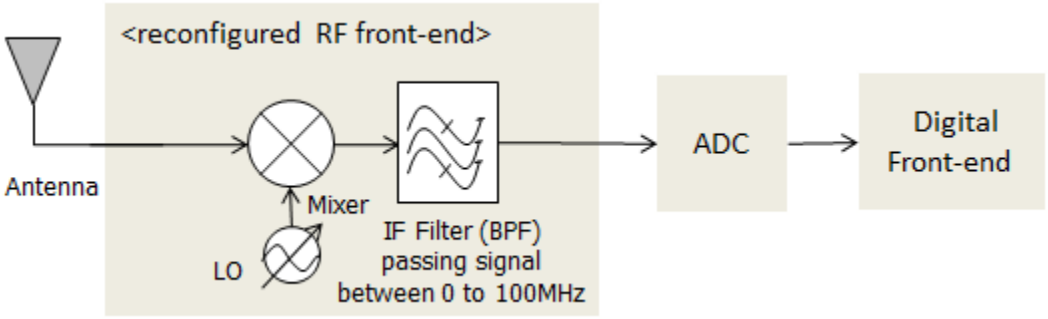

Figure 3.2: Spectrum Analyzer - reconfigurable RF front-end has a configuration that bypasses all filters and amplifiers and has a homodyne architecture.

3.2 Environment-Adaptable Fast (EAF) Optimization

The EAF optimization is designed to solve the reconfigurable RF front-end optimization problem in (1.1). In this thesis, we define the cost function $F(\mathbf{x})$ as the power consumption of the configuration $\mathbf{x}$, and we consider a single constraint function $g(\mathbf{x}, t)$, defined as the measured SINR. Thus, the optimization problem considered in this thesis is as below:

$$\begin{aligned} \mathbf{x}^{(opt)} = \quad & arg\min \quad \text{Power}(\mathbf{x}), \\ & \text{SINR}(\mathbf{x}, t) \geq \text{SINR}_{\text{spec}} \end{aligned} \tag{3.14}$$

where $\text{SINR}_{\text{spec}}$ is the minimum SNR acceptable for adequate system performance.

3.2.1 EAF Optimization Design

The EAF optimization method is composed of two phases as shown in Figure 3.3. This algorithm is an adaptation of the Two-phase relaxation algorithm proposed in [19].

Algorithm 4 The Two-phase Algorithm (Phase I): find the configuration $\mathbf{x}^{(max)}$ of the highest $\text{SINR}^{(max)}$ in all configurations.

$\text{SNR}_{\text{calc}}{}^{(max)} \leftarrow \text{SNR}^{(init)}$.
$\mathbf{x}^{(max)} \leftarrow \mathbf{x}^{(init)}$
for $k = 1, 2, \cdots, K$ **do**
    $\mathbf{x}^{(k)} \leftarrow$ the k-th configuration
    $\text{SNR}^{(k)} \leftarrow$ calculated SINR of $\mathbf{x}^{(k)}$
    if $\text{SNR}^{(k)} > \text{SNR}^{(max)}$ **then**
        $\mathbf{x}^{(max)} \leftarrow \mathbf{x}^{(k)}$
        $\text{SNR}_{\text{calc}}{}^{(max)} \leftarrow \text{SNR}^{(k)}$
    end if
end for
$\text{SNR}^{(max)} \leftarrow$ simulated (or measured) SINR of $\mathbf{x}^{(k)}$
OUTPUT: $\mathbf{x}^{(max)}$, $\text{SNR}^{(max)}$

In the first phase (Phase I), the EAF optimization finds $\mathbf{x}^{(max)}$ as a configuration which has the *highest calculated SINR* value among all available configurations. Finding $\mathbf{x}^{(max)}$

directly from SINR calculation significantly reduces computational cost. This is because finding a point of the maximal SINR iteratively is the most time-consuming process in the optimization process. The pseudocode of Phase I is given in Algorithm 4, where $\mathbf{x}^{(k)}$ is the k-th configuration and $\text{SNR}^{(k)}$ is the calculated SINR of $\mathbf{x}^{(k)}$.

In the second phase (Phase II), the EAF optimization utilizes the calculated SINR to search for a configuration of the lowest power that still satisfies the SINR specification for a given communication standard. By looking up the calculated SINR, we were able to discern and prune out configurations that likely do not meet the SINR specification. In other words, we excluded configurations $\mathbf{x}^{(k)}$ that do not satisfy the constraint function $\text{SINR}^{(k)} \geq$ (SINR threshold) in the optimization process. The details of the proposed op-

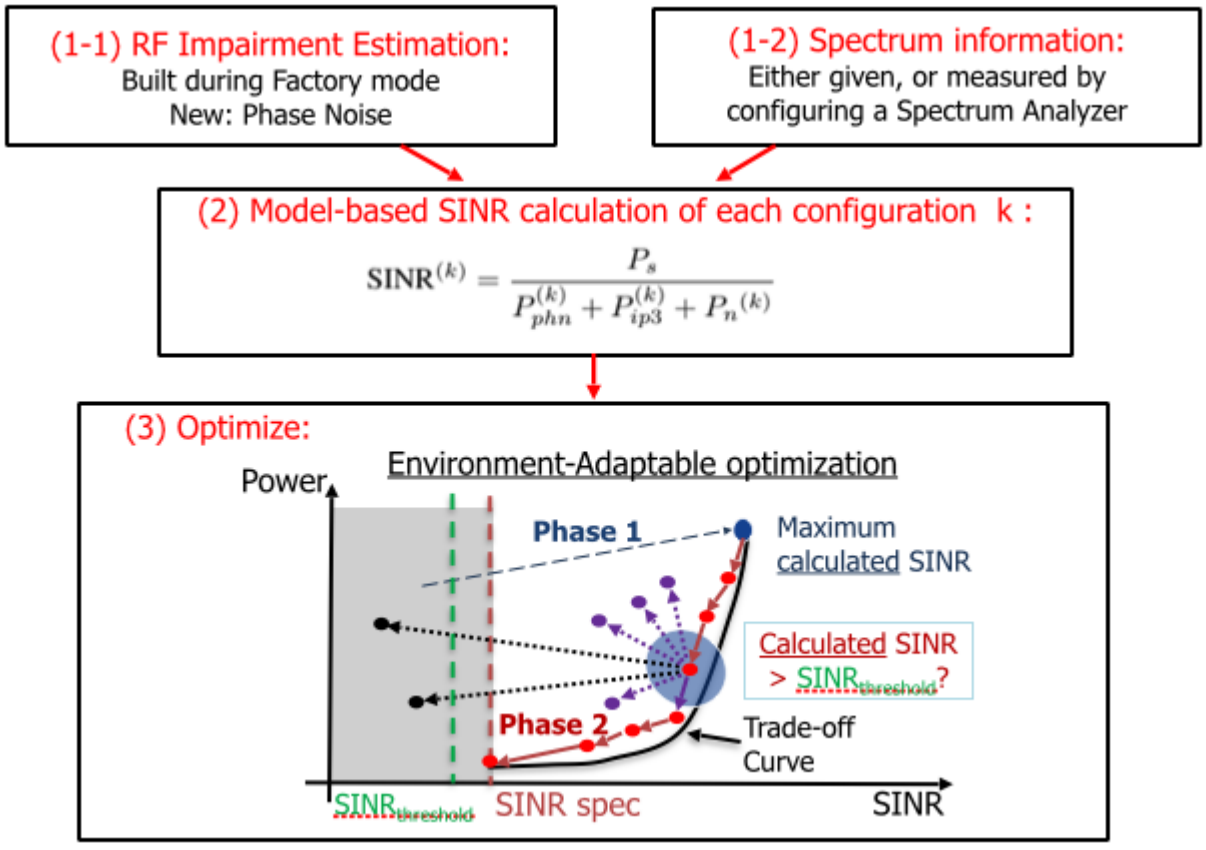

Figure 3.3: Flow Chart of the EAF Optimization Algorithm.

timization method are given as pseudo-code in Algorithm 5. Thus, the SINR calculation can minimize the search space of overall configurations, and the EAF optimization can drop its computational cost.

Algorithm 5 The Two-phase Algorithm (Phase II): find an optimal configuration $\mathbf{x}^{(opt)}$

1: INPUT: $\mathbf{x}^{(max)}$, SNR$^{(max)}$
2: $\mathbf{x}^{(current)} \leftarrow \mathbf{x}^{(max)}$
3: SINR$^{(current)} \leftarrow$ SNR$^{(max)}$
4: $\mathbf{x}^{(old)} \leftarrow \mathbf{x}^{(current)}$
5: **for** $m = 1, 2, \cdots, M$ **do**
6: **for** $n = 1, 2, \cdots, N_m$ **do**
7: $\mathbf{x}^{(current)} \leftarrow \mathbf{x}_m(n)$
8: SINR$^{(current)} \leftarrow$ calculated SINR of $\mathbf{x}^{(current)}$
9: **if** SINR$^{(current)} <$ SINR$_{\text{threshold}}$ **then**
10: continue
11: **else**
12: SINR$^{(current)} \leftarrow$ simulated (or measured) SINR for $\mathbf{x}^{(current)}$
13: Power$^{(current)} \leftarrow$ power of $\mathbf{x}^{(current)}$
14: **end if**
15: **if** SINR$^{(current)} \geq$ SINR$_{\text{spec}}$ **then**
16: $E_m(n) =$ Power$^{(current)}$
17: **else**
18: $E_m(n) = \infty$
19: **end if**
20: **end for**
21: $\mathbf{x}^{(new)} = \underset{\mathbf{x} \in \{\mathbf{x}_m(n) | n=1,2,\cdots,N_m\}}{\arg\min} E_m(n)$
22: **if** $\mathbf{x}^{(new)} = \mathbf{x}^{(old)}$ **then**
23: break
24: **else**
25: $\mathbf{x}^{(old)} \leftarrow \mathbf{x}^{(new)}$
26: **end if**
27: **end for**
28: $\mathbf{x}^{(opt)} \leftarrow \mathbf{x}^{(old)}$
29: OUTPUT: $\mathbf{x}^{(opt)}$

If there are M RF components connected serially in a reconfigurable RF front-end, the variable m in line 5 refers to the m-th RF component, such as amplifiers, filters, and

mixers. We can write the configuration $\mathbf{x} = [x_1, x_2, \cdots, x_m, \cdots, x_M]$ where x_m refers to the m-th component selection. For the m-th RF component, there are N_m configurations such as amplifier1, amplifier2, etc. The variable n in line 6 represents the n-th configuration of the given m-th RF component. For the current configuration $\mathbf{x}^{(current)}$, $\mathbf{x}_m(n)$ in line 7 is the configuration that chooses the n-th available component value at the m-th RF component. Therefore, using the proposed algorithm, we find the (locally) optimal configuration $\mathbf{x}^{(opt)}$ of the optimization problem in (3.14).

3.2.2 Simulation Results

In this section, the performance of the designed EAF optimization is compared with four other previously proposed optimization methods, and its efficiency is verified by simulation using Matlab Simulink with the SimRF toolbox.

Simulation Setup

The RF receiver is designed for the IEEE 802.11g WLAN standard where the carrier frequency is 2.4 GHz and the channel bandwidth is 20 MHz. While the received signal has a power of -65 dBm, a narrowband blocker has a power of -35 dBm at 2.42 GHz. In this example, the reconfigurable RF front-end is reconfigured by switching three amplifiers and one oscillator, as shown in Figure 1.2 (b). The banks of three amplifiers have six possible configurations each. One oscillator has five possible configurations. Thus, there are a total of 1080 different candidate configurations for the reconfigurable RF front-end. $\text{SINR}_{\text{spec}} = 29$ (dB) was used for the optimization problem.

Simulation Results

In order to demonstrate its performance, we compare our proposed environment-adaptable fast (EAF) optimization method with the four algorithms proposed in [6].

(1) Exhaustive search: All configurations are simulated one by one, and based on the obtained SINR, the exhaustive search method finds the optimal configuration.

(2) Local relaxation search: In each iteration, only one RF component in a current configuration can be adaptable to possible component values from a bank, while other RF components are fixed. A local optimum among the simulated configurations is updated to the current configuration for the next iteration.

(3) Simulated annealing search: In each iteration, the random neighbor configurations of a current configuration can be simulated by changing possible configurations in a bank. A local optimum among the simulated neighbor configurations is stochastically updated to the current configuration for the next iteration.

(4) Two-phase relaxation search [19]: The two-phase relaxation search first narrows down the search space of configuration using a Pareto optimal front. In the first phase, using a local relaxation search, this method searches a configuration of maximal SNR, which is the initial point for the second phase. In the second phase, it searches a configuration of minimum power, while satisfying the SINR constraint.

(5) EAF optimization: This method is explained in Section 3.2.1.

In Table 3.1, the performance of the EAF optimization algorithm is compared to the

Table 3.1: Programming Results for the Reconfigurable RF Front-end

Algorithm	SNR (dB)	Power (mW)	No. Simulation Steps
(1) Exhaustive	30.5	71.7	1080
(2) Local Relaxation	29.4	96.8	12
(3) Simulated Annealing	30.5	71.7	293
(4) Two-phase [19]	31.2	99.5	26
(5) EAF optimization [6]	31.2	99.5	5

performance of the other four optimization methods. We set the SINR threshold to 24 dB in the EAF optimization to conservatively accept candidate configurations because $\text{SINR}_{\text{spec}} = 29$ (dB).

(1) The exhaustive optimization finds a global optimal configuration, but it is time-consuming with 1080 simulation steps. (2) The local relaxation search finds a local optimal configuration. This method is more practical compared to the exhaustive search as it takes only 12 simulation steps. (3) The simulated annealing optimization takes 293 simulation steps - it is more efficient than the exhaustive search, but still takes many more steps than the local relaxation search. Still, the simulated annealing optimization is able to find the global optimum. (4) The Two-phase relaxation search finds a local optimal configuration with slightly higher SINR than the local relaxation search. This method has more than twice the number of simulation steps than the local relaxation search. It takes longer because of the additional first phase of finding a configuration of maximum SINR.

(5) Finally, the EAF optimization method is the fastest of the five methods. This method takes five simulation steps, and the SINR and power of the optimal configuration is similar to the two-phase optimization. In Table 3.2, Phase I of the EAF optimization needs only one simulation step compared with 19 simulation steps of the Two-phase relax-

ation optimization method. Phase II of the EAF optimization takes four simulation steps while Phase II of the Two-phase relaxation optimization needs seven simulation steps. In both Phase I and Phase II, calculated SINR significantly helps reduce the number of simulation steps. Therefore, we can verify that the EAF optimization method significantly improves computational cost compared to the other four optimization methods, and it can still find a configuration with acceptable performance.

Table 3.2: The Number of Simulation Steps for the Reconfigurable RF Front-end

Algorithm	Phase I	Phase II	Phase 1 + Phase II
(4) Two-phase [19]	19	7	26
(5) EAF optimization [6]	1	4	5

In this chapter, we introduced our EAF optimization method and verified it on a small-scale RF front-end. While our method shows potential to improve the efficiency of optimization, we need to apply our method to a more realistic large-scale RF-FPGA system. This is the subject of Chapter 4.

Chapter 4

EAF Optimization in Large-scale RF-FPGA Systems

In Section 3.2, we showed that our EAF optimization method can be successfully utilized as a heuristic to find a minimum power configuration of adequate SNR in an experimental case of a (small) reconfigurable RF system. In contrast, a realistic RF-FPGA is likely to be controlled by several hundred bits that select the component values. Such a large-scale RF-FPGA poses a significant problem for EAF optimization because it is not possible to directly measure and characterize the RF impairments of each of the possible configurations. In this chapter, we investigate a model-based approach to solve this problem, allowing the use of EAF optimization in large-scale RF-FPGA systems.

4.1 RF Impairment Estimation in Large-scale RF-FPGA Systems

In this section, we investigate the estimation of RF impairments in a large-scale RF front-end. The first problem associated with this large-scale is that the large number of RF front-ends span a wide range of RF impairment values. In Section 4.1.1, we solve this problem by designing a method that adjusts the transmission power during the estimation procedure. The second problem is the large number of configurations in a large-scale RF front-end. This problem is tackled by using a Design of Experiments (DoE) approach and an Interpolation procedure as discussed in Section 4.1.2. These methods are important in a large-scale RF front-end because we cannot simulate (or estimate) all configurations; we can only simulate a limited number of sample configurations. For example, a reconfigurable RF front-end with 63 bits of control means that the number of configurations is about 9.2×10^{18}, which results in an impractically time-consuming estimation procedure. Our methods of RF impairment estimation in a large-scale RF front-end are utilized to efficiently extract unknown properties of RF components from known properties that are calculated from simulated data. This method of RF impairment estimation is applied to a large-scale RF front-end of 63 bits.

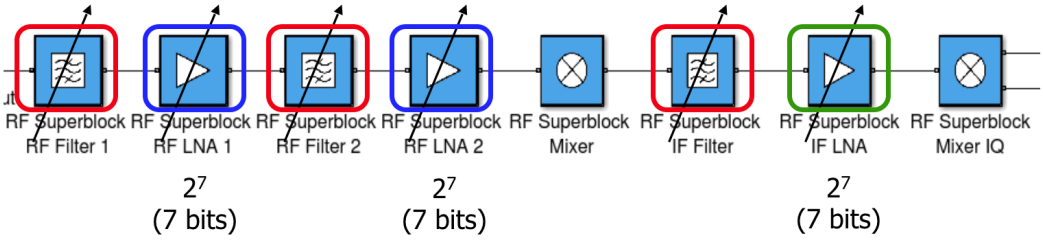

Figure 4.1: A large-scale RF-FPGA system with 63 bits of control.

4.1.1 Tackling a Wide Range of RF Impairment Values: Bias in IIP_3 Estimate

Consider a large-scale RF-FPGA system, as shown in Figure 4.1. This front-end has 63 bits of control, allowing a wide range of values for gain and IIP_3. Due to this, configurations with a wide range of IIP_3 values are possible. Figure 4.2 shows that the wide range of IIP_3 results in bias in estimated IIP_3. Specifically, we found two areas of large bias: lower boundary around -65 dBm and upper boundary around -43 dBm. The wide range within the estimated IIP_3 from -80 dBm to -10 dBm is mainly due to high gains obtained by passing through multiple amplifiers. In order to solve the bias (saturation) problem in IIP_3 estimation, we obtained a formula for adjusting transmission power to a RF front-end. The transmission power P_{tx} was derived from the upper and lower boundaries of IIP_3 saturation.

The upper boundary of IIP_3 saturation is related to thermal noise. Thermal noise power should be smaller than the Intermodulated signal power of transmitted signals in order to be detected during the estimation procedure. More specifically, the overall thermal noise power after passing a reconfigurable RF front is given as $NF_{0(dBm/Hz)} + \Delta f_{(dB)} + NF_{(dB)}$ where thermal noise floor is $NF_{0(dBm/Hz)} = -174(dBm/Hz)$, $\Delta f_{(dB)} = 10 \cdot log_{10} B_{(dB)}$ for the bandwidth $B_{(Hz)}$ of the transmitted signal, and $NF_{(dB)}$ is an additional noise figure for noise margin. Meanwhile, the intermodulated signal with IIP_3 has a power of $3 \cdot P_{\text{sig}(dBm)} - 2 \cdot \text{IIP}_{3(dBm)}$ where P_{sig} is the nominal transmitted signal power of the two transmitted signals that are intermodulated. So, we derive the following condition to allow accurate estimation of IIP_3.

$$NF_{0(dBm/Hz)} + \Delta f_{(dB)} + NF_{(dB)} < 3 \cdot P_{\text{sig}(dBm)} - 2 \cdot \text{IIP}_{3(dBm)}, \tag{4.1}$$

where $\Delta f_{(dB)} = 10 \cdot log_{10} B_{(dB)}$.

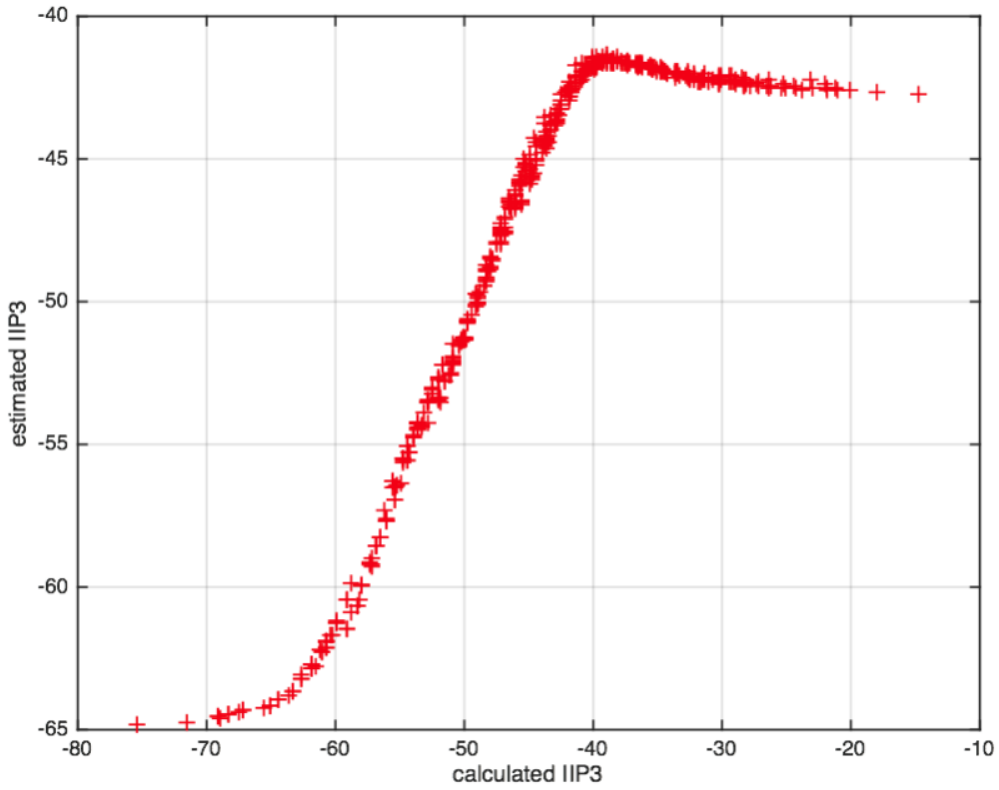

Figure 4.2: Calculated IIP_3 from library data is given on the x-axis and estimated IIP_3 from simulation is given on the y-axis when three amplifiers are reconfigured in a reconfigurable RF front-end. There are two saturation areas according to where the IIP_3 estimate is: the lower boundary around -65 dBm and the upper boundary around -42 dBm IIP_3.

From this, the upper boundary of IIP_3 saturation is given as,

$$\begin{aligned} \text{IIP}_{3(dBm)} &< \frac{1}{2}\left(3 \cdot P_{\text{sig}(dBm)} - \left(NF_{0(dBm/Hz)} + \Delta f_{(dB)} + NF_{(dB)}\right)\right) \\ &= P_{\text{sig}(dBm)} + \frac{1}{2}\left(P_{\text{sig}(dBm)} - \left(NF_{0(dBm/Hz)} + \Delta f_{(dB)} + NF_{(dB)}\right)\right) \end{aligned} \quad (4.2)$$

The lower boundary of IIP_3 saturation in Figure 4.2 is related to the transmitted signal power P_{sig}. A transmitted signal with a high power level suffers from nonlinearity intermodulation. When an intermodulated signal by the third order nonlinearity has a power

as large as the power of a transmitted sinusoid, the transmission power is defined as IIP_3. Thus, the transmitted signal power P_{sig} should be smaller than IIP_3 as follows,

$$P_{\text{sig}(dBm)} < \text{IIP}_{3(dBm)}. \tag{4.3}$$

From (4.2) and (4.3), the range of IIP_3 over which we can expect low bias is given as,

$$K_0 < \text{IIP}_{3(dBm)} < K_0 + \Delta K, \tag{4.4}$$

where $K_0 = P_{\text{sig}(dBm)}$ and $\Delta K = \frac{1}{2}\left(P_{\text{sig}(dBm)} - \left(NF_{0(dBm/Hz)} + \Delta f_{(dB)} + NF_{(dB)}\right)\right)$.

Now we specify the choice of transmission power $P_{\text{tx}(dBm)} = P_{\text{sig}(dBm)} + \Delta P_{(dB)}$ that should be used for IIP_3 estimation to allow low bias.

The overall IIP_3 of a configuration of cascaded components is as follows,

$$\frac{1}{\text{IIP}_3} = \frac{1}{\text{IIP}_{3,1}} + \frac{G_1}{\text{IIP}_{3,2}} + \cdots + \frac{G_1 \cdot G_2 \cdot \cdots \cdot G_{N-1}}{\text{IIP}_{3,N}}, \tag{4.5}$$

where $\text{IIP}_{3,k}$, G_k are the IIP_3 and gain of the k-th component for $k = 1, 2, \cdots, N$.

From this, we can assume that the nonlinearity of the last cascaded component is dominant, i.e., $\frac{1}{\text{IIP}_3} \approx \frac{G_1 \cdot G_2 \cdot \cdots \cdot G_{N-1}}{\text{IIP}_{3,N}}$. In that case, IIP_3 is given as $\text{IIP}_{3(dBm)} \approx \text{IIP}_{3,N(dBm)} - {G_1^{N-1}}_{(dB)}$ where G_1^{N-1} is the overall gain of the first $N-1$ components: ${G_1^{N-1}}_{(dB)} = G_{1(dB)} + G_{2(dB)} + \cdots + G_{N-1(dB)}$.

Thus, (4.4) is given as in terms of the IIP_3 of the last component,

$$K_0 + {G_1^{N-1}}_{(dB)} < \text{IIP}_{3,N(dBm)} < K_0 + \Delta K + {G_1^{N-1}}_{(dB)}. \tag{4.6}$$

Now, we assume that the approximate range of IIP_3 such as ${\text{IIP}_{3,N}}^{(min)}$ and ${\text{IIP}_{3,N}}^{(max)}$ of (the last) component is known. We define the transmission power increase ΔP over the nominal value $P_{\text{sig}(dBm)}$ for use in IIP_3 estimation. Then, the range of power increase ΔP that satisfies (4.6) is given as follows,

$$
\begin{aligned}
\Delta P^{(max)}{}_{(dB)} &= \text{IIP}_{3,N}{}^{(min)}{}_{(dBm)} - (K_0 + G_1^{N-1}{}_{(dB)}) \\
\Delta P^{(min)}{}_{(dB)} &= \text{IIP}_{3,N}{}^{(max)}{}_{(dBm)} - (K_0 + \Delta K + G_1^{N-1}{}_{(dB)}).
\end{aligned} \tag{4.7}
$$

Thus, we choose ΔP to be the mean of $\Delta P^{(max)}{}_{(dB)}$ and $\Delta P^{(min)}{}_{(dB)}$ in order to avoid IIP_3 estimation saturation.

$$
\begin{aligned}
\Delta P_{(dB)} &= \text{mean}(\Delta P^{(max)}{}_{(dB)}, \Delta P^{(min)}{}_{(dB)}) \\
&= 0.5 \cdot (\text{IIP}_{3,N}{}^{(min)}{}_{(dBm)} + \text{IIP}_{3,N}{}^{(max)}{}_{(dBm)}) \\
&\quad -K_0 - 0.5 \cdot \Delta K - G_1^{N-1}{}_{(dB)}.
\end{aligned} \tag{4.8}
$$

Thus, in a large-scale RF front-end, the transmission power P_{tx} for IIP_3 estimation is given as,

$$
\begin{aligned}
P_{\text{tx}(dBm)} &= P_{\text{sig}(dBm)} + \Delta P_{(dB)} \\
&= 0.5 \cdot (\text{IIP}_{3,N}{}^{(min)}{}_{(dBm)} + \text{IIP}_{3,N}{}^{(max)}{}_{(dBm)}) \\
&\quad -0.5 \cdot \Delta K - G_1^{N-1}{}_{(dB)}.
\end{aligned} \tag{4.9}
$$

4.1.2 Tackling a Large Number of Configurations: Design of Experiments (DoE) and Interpolation Methods

A significant challenge in applying the EAF optimization method to a large-scale RF front-end is that RF impairment estimation is time-consuming when the number of configurations is very large. In this section, we use model-based Design of Experiments (DoE) and Interpolation methods to drastically reduce the time needed for estimation.

Configuration Subsets: Full-factorial Design Set, Screening Design Set and Sample Configuration Set

The configurations of a large-scale RF front-end can be successively narrowed into the following subsets: full-factorial design set, screening design set, and sample configuration set as shown in Figure 4.3. First, a full-factorial design set includes all possible configurations for a large-scale RF front-end. In our example in Figure 4.1, assuming three fixed filters and three reconfigurable amplifiers that are composed of three 7-bit sub-amplifiers, the set of full-factorial design has configurations with 63 bits of control. A screening design set is a subset of the full-factorial design set, and includes the most significant factors of configurations. The configurations of a screening design set are obtained by reconfiguring only a few of the most significant bits (MSBs) of sub-amplifiers as seen in Figure 4.4. In our example, two MSBs of three sub-amplifiers are allowed to be reconfigured with the remaining bits held constant at 0, resulting in a screening design set of configurations with 18 bits of control. Finally, sample configurations are selected for actual simulation and data collection from within the screening design set.

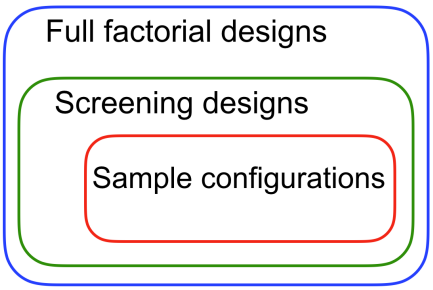

Figure 4.3: Configuration subsets - full-factorial design set, screening design set and sample configuration set.

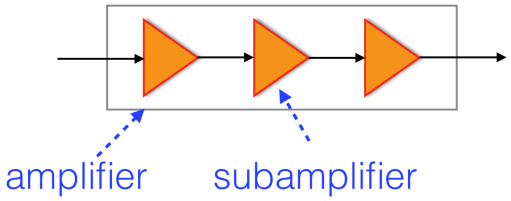

Figure 4.4: Three sub-amplifiers in an amplifier- In our example, two MSBs of three sub-amplifiers are allowed to be reconfigured for a screening design set.

Configuration Subsets and RF Impairment Calculation

In a cascaded chain of RF components, as in Figure 4.1, we can calculate the overall RF impairment from the component values using the following formula,

$$G^A{}_{(dB)} = G_{1(dB)} + G_{2(dB)} + \cdots + G_{N(dB)}, \tag{4.10}$$

$$\frac{1}{\text{IIP}_3{}^A} = \frac{1}{\text{IIP}_{3,1}} + \frac{G_1}{\text{IIP}_{3,2}} + \cdots + \frac{G_1 \cdot G_2 \cdot \cdots \cdot G_{N-1}}{\text{IIP}_{3,N}}, \tag{4.11}$$

$$F^A - 1 = F_1 - 1 + \frac{F_2 - 1}{G_1} + \frac{F_3 - 1}{G_1 \cdot G_2} + \cdots + \frac{F_N - 1}{G_1 \cdot G_2 \cdot \cdots \cdot G_{N-1}}, \tag{4.12}$$

where G_k, $\text{IIP}_{3,k}$, and F_k are the gain, IIP_3, and noise factor, respectively, of the k-th component of a configuration ($k = 1, 2, \cdots, N$), and G^A, $\text{IIP}_3{}^A$, and F^A are the overall gain, IIP_3, and noise factor, respectively, of the configuration.

Thus, in order to obtain an unknown value of overall RF impairments, we need to obtain the component values of RF impairments. We will now explain how to obtain component values from sample configurations and how to select sample configurations based on a linear model of RF components in Section 4.1.2.

Linear Model of RF Impairments in a Large-scale RF-FPGA

We note that, perhaps surprisingly, (4.10), (4.11) and (4.12) are all of the same general linear form,

$$Z = h_1 X_1 + h_2 X_2 + \cdots + h_k X_k + \cdots + h_N X_N, \tag{4.13}$$

where X_k represents the RF impairment of the k-th component of a configuration, h_k is a coefficient for the k-th term, $k = 1, 2, \cdots, N$, and Z represents the overall RF impairment of the configuration. The impairment can be either gain ($X_k = G_{k(dB)}$), IIP_3 ($X_k = 1/\text{IIP}_3$), or noise factor ($X_k = F_k - 1$). For example, for (4.11), $X_k = \dfrac{1}{\text{IIP}_{3,k}}$, $h_1 = 1$, $h_k = G_1 \cdot G_2 \cdot \cdots \cdot G_{k-1}$, for $k \in \{2, \cdots, N\}$.

When the value of the k-th component X_k is chosen in a set of component values, $\{\theta_{k,1}, \theta_{k,2}, \cdots, \theta_{k,C_k}\}$, we can define the vector θ that is composed of all available component values as follows,

$$\theta = \Big[\underbrace{\theta_{1,1}, \theta_{1,2}, \cdots, \theta_{1,C_1}}, \underbrace{\theta_{2,1}, \theta_{2,2}, \cdots, \theta_{2,C_2}}, \cdots, \underbrace{\theta_{N,1}, \theta_{N,2}, \cdots, \theta_{N,C_N}}\Big]^T. \tag{4.14}$$

Then, we can build a linear model,

$$\mathbf{Y} = \mathbf{H} \cdot \theta + \mathbf{N}, \tag{4.15}$$

where $\mathbf{Y}$ is the vector of measured RF impairment using simulation or actual measurement (each element corresponding to one sample configuration that is simulated) while the vector $\mathbf{N}$ represents measurement noise during the estimation process.

We will now present how to define the matrix $\mathbf{H}$ in (4.15). The k-th component X_k in (4.13) chooses a component value $\theta_{k,k'}$ in (4.14) ($k' \in \{1, 2, 3, \cdots, C_k\}$), and (4.13) is

given as follows,

$$\begin{aligned} Y &= h_1\theta_{1,1'} + h_2\theta_{2,2'} + \cdots + h_k\theta_{k,k'} \cdots + h_N\theta_{N,N'} + N \\ &= [h_1 \cdot \mathbf{g}_1, h_2 \cdot \mathbf{g}_2, \cdots, h_k \cdot \mathbf{g}_k, \cdots, h_N \cdot \mathbf{g}_N] \cdot \theta \\ &= \mathbf{h}' \cdot \theta \end{aligned} \tag{4.16}$$

where the row sub-vector $\mathbf{g}_k$ in $\mathbf{h}'$ is defined as follows,

$$(\mathbf{g}_k)_{1,l} = \begin{cases} 1 & \text{if } l = k' \\ 0 & \text{otherwise,} \end{cases} . \tag{4.17}$$

where $l = 1, 2, 3, \cdots, C_k$.

Thus, we can define the matrix $\mathbf{H}$ in (4.15) composed of the row vector $\mathbf{h}'$ in (4.16) corresponding to the measured sample configuration Y.

Based on (4.15), we obtain the unknown characteristics $\widehat{\theta}$ of all components using Least-Squares (LS) estimation as below,

$$\widehat{\theta} = (\mathbf{H}^T \cdot \mathbf{H})^{-1} \cdot \mathbf{H} \cdot \widehat{\mathbf{Y}}. \tag{4.18}$$

Given any configurations with unknown RF impairment, we can use (4.13) to estimate its impairment using the estimated component values $\widehat{\theta}$. Thus, using a screening design set of sample configurations, we can estimate component values $\widehat{\theta}$ and use the method (4.13) to predict the RF impairments of any configurations as shown in Figure 4.5.

Design of Experiments (DoE) for Choosing Optimal Sample Configurations

We select a set of *optimal* sample configurations among the configurations in the screening design set using the Design of Experiments (DoE) approach. The DoE method selects an optimal set of sample configurations (equivalently, the matrix $\mathbf{H}$ in (4.18) corresponding to the selected sample configurations) using a D-optimal design approach. The D-optimal design approach iteratively updates a set of configurations in order to increase

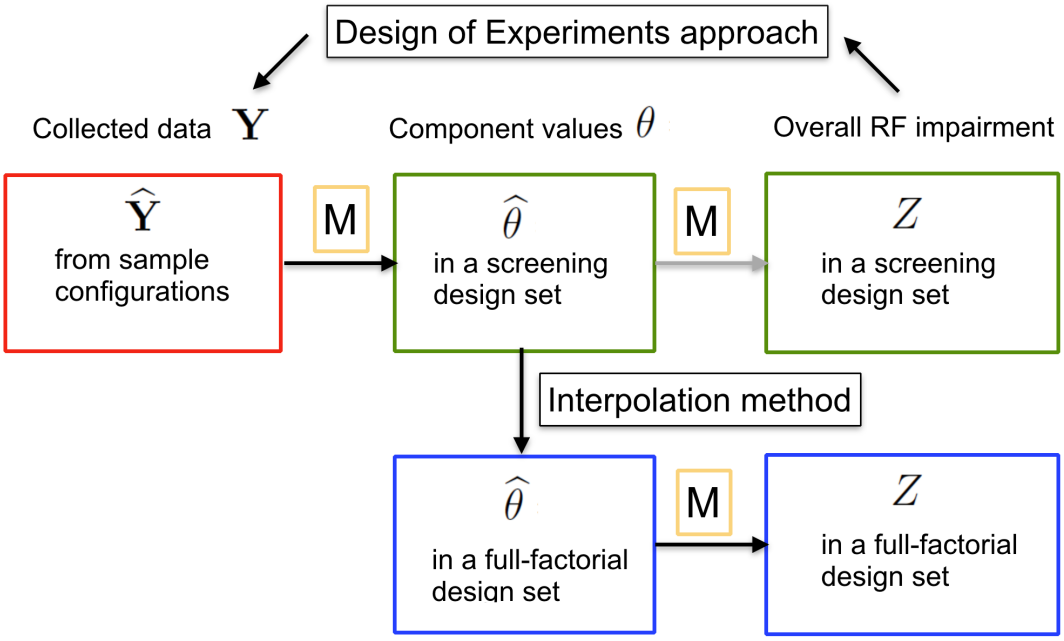

Figure 4.5: Design of Experiments (DoE) and Interpolation Methods for Tackling a Large Number of Configurations.

the determinant $|\mathbf{H}^T \cdot \mathbf{H}|$ i.e., minimize the log-determinant of noise variance matrix in (4.15) to find optimal sample configurations. The implementation details of the DoE method for choosing sample configurations are described in Algorithm 6.

Algorithm 6 The DoE Approach: find $\mathbf{X}_{\text{DoE}}$ (a set of sample configurations) and a matrix $\mathbf{H}_{\text{DoE}}$ in (4.15).

1: INPUT: m, $\mathbf{X}_{\text{Screening}}$
2: $N_{\text{condition}} = \infty$ ▷ conditional number
3: $\mathbf{H}_{\text{Screening}} = function_{\text{amplifier ID to } \mathbf{H}}\left(\mathbf{X}_{\text{Screening}}\right)$
4: **while** $N_{\text{condition}} > {N_{\text{condition}}}^{(threshold)}$ **do**
5: $l_X = function_{\text{d-optimal method}}\left(m, \mathbf{H}_{\text{Screening}}\right)$ ▷ a list of the extracted rows of $\mathbf{X}_{\text{Screening}}$
6: $\mathbf{H}_{\text{DoE}} = \mathbf{H}_{\text{Screening}}(l_X, :)$
7: $\mathbf{X}_{\text{DoE}} = \mathbf{X}_{\text{Screening}}(l_X, :)$ ▷ a row matrix of sample configurations
8: $\lambda^{(max)} \leftarrow$ the maximum of eigenvalues of ${\mathbf{H}_{\text{DoE}}}^T \cdot \mathbf{H}_{\text{DoE}}$
9: $\lambda^{(min)} \leftarrow$ the minimum of eigenvalues of ${\mathbf{H}_{\text{DoE}}}^T \cdot \mathbf{H}_{\text{DoE}}$
10: $N_{\text{condition}} = \lambda^{(max)}/\lambda^{(min)}$
11: **end while**
12: OUTPUT: $\mathbf{X}_{\text{DoE}}, \mathbf{H}_{\text{DoE}}$

In line 1, m is the number of sample configurations to be selected. $\mathbf{X}_{\text{Screening}}$ is a row matrix composed of all configurations in a screening design set that is obtained by reconfiguring a few pre-defined MSBs of sub-amplifiers. In line 3, $\mathbf{H}_{\text{Screening}}$ is the matrix $\mathbf{H}$ in (4.15) corresponding to $\mathbf{X}_{\text{Screening}}$. In line 4, ${N_{\text{condition}}}^{(threshold)}$ is a constant of the maximal limit of condition number $N_{\text{condition}}$. In line 5, l_X is a list of m selected rows of $\mathbf{X}_{\text{Screening}}$ for sample configurations.

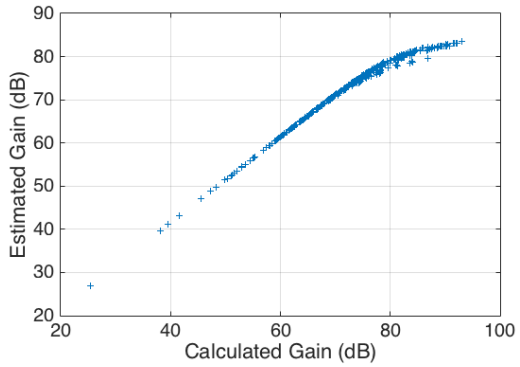

(a) Estimated gain $\widehat{\mathbf{Y}}$ of configurations in a sample configuration set

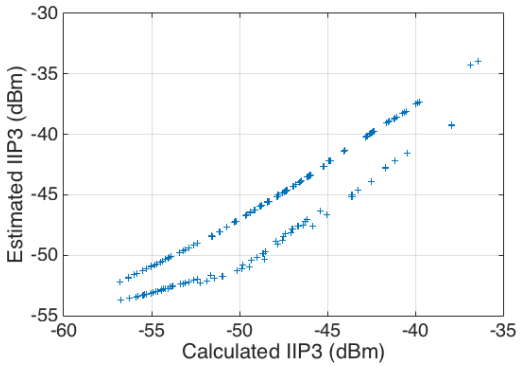

(b) Estimated IIP_3 $\widehat{\mathbf{Y}}$ of configurations in a sample configuration set

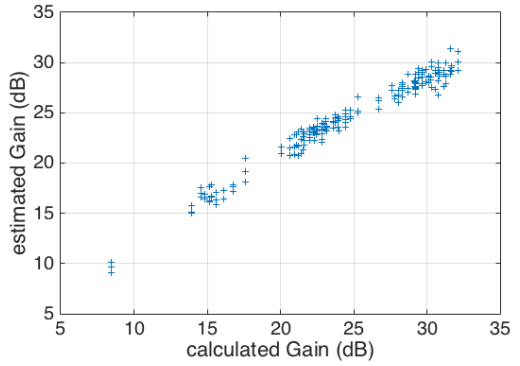

(c) Estimated gain $\widehat{\theta}$ of each amplifier

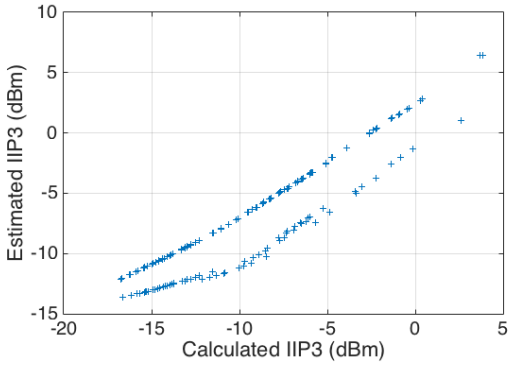

(d) Estimated IIP_3 $\widehat{\theta}$ of each amplifier

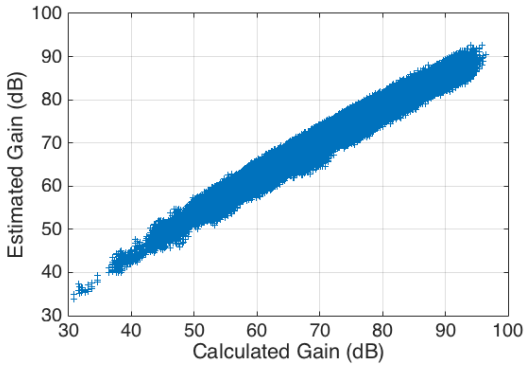

(e) Estimated gain $\widehat{\mathbf{Z}}$ of configurations in a screening design set

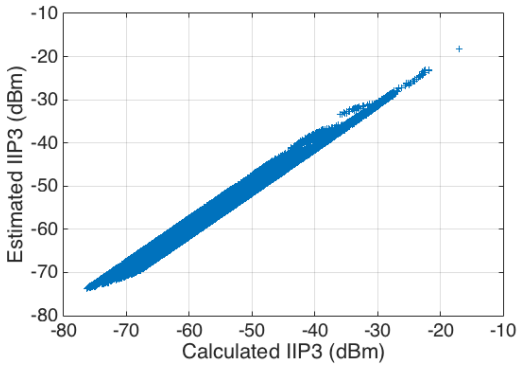

(f) Estimated IIP_3 $\widehat{\mathbf{Z}}$ of configurations in a screening design set

Figure 4.6: Simulation Results for RF impairment estimation using the Design of Experiments (DoE) method.

Simulation Results

Figure 4.6 shows the simulation results of gain and IIP_3 estimation by applying the DoE method to the RF-FPGA (Figure 4.1). We verify that the method can be successfully used to estimate RF impairments of any configuration using a model-based approach, with component values estimated by a DoE method.

The estimated gain and IIP_3, $\widehat{Y}$ in (4.18), of sample configurations are plotted on the y-axis against true gain and IIP_3 Y of the sample configurations on the x-axis in Figure 4.6a and 4.6b respectively. The simulation results show that the estimates of $\widehat{Y}$ proportionally increase with true values of $\widehat{Y}$. (At high gain values, around 100 dB, the estimates begin to saturate in Figure 4.6a. Also, configurations where at least one amplifier is bypassed have IIP_3 estimates which are about 3 dB lower in Figure 4.6b.)

The estimated gain and IIP_3, $\widehat{\theta}$ of the three amplifiers, are plotted on the y-axis against true gain and IIP_3 θ of the three amplifiers on the x-axis in Figure 4.6c and 4.6d respectively. The estimates $\widehat{\theta}$ proportionally increase with true values of θ. (The estimated IIP_3 of the first and second amplifiers are about 3 dB lower than that of the third amplifier in Figure 4.6d.)

Finally, the estimated gain and IIP_3, $\widehat{\mathbf{Z}}$, of the remaining configurations in the screening design set are plotted on the y-axis against true gain and IIP_3 $\mathbf{Z}$ on the x-axis in Figure 4.6e and 4.6f respectively. The estimates $\widehat{\mathbf{Z}}$ proportionally increase with true values of $\mathbf{Z}$.

Interpolation Method

In order to extend the RF impairments estimated for configurations in the screening design set to the full-factorial design set, the interpolation method is applied. Recollect that the configurations in the screening design set only use a few of the MSB bits of each component, with the other bits frozen to zero. The assumption made here is that the bits of each component define a real number (or set of real numbers) and that the true RF impairment is a continuous function of this (set of) real numbers.

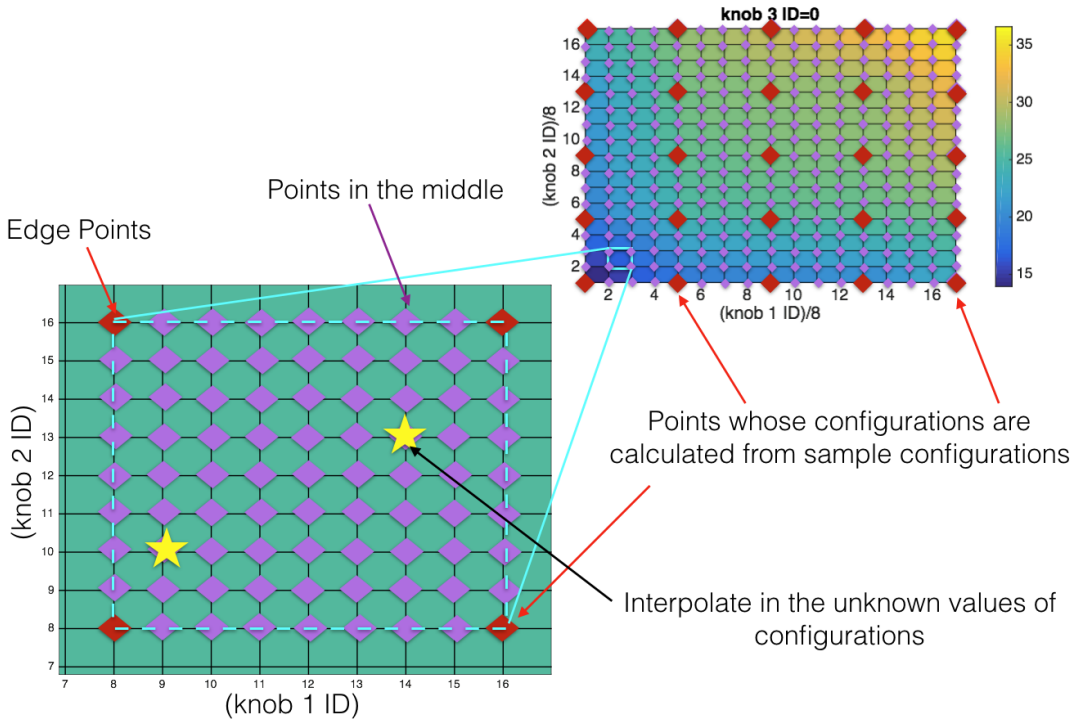

Figure 4.7: The interpolation method is applied to obtain information of the configurations with known RF impairments from the configurations with unknown RF impairments.

The red data points - the configurations in a screening design set - have identified values $\widehat{\theta}$ in (4.18) obtained from the sample configurations as described in Section 4.1.2.

The stared points - the configurations in a full factorial design set - have unknown but identifiable values by applying the interpolation method. First, the parameters in a mathematical model are determined to fit data of configurations in a screening design set to the mathematical model. Second, using the parameters and the mathematical model, the interpolation method interpolates the unknown component values in configurations. The pseudocode of the interpolation method is given in Algorithm 7. For the interpolation process, we utilized the Natural neighbor interpolation. Simulation results of applying the interpolation method are plotted in Figure 4.8. Thus, we could measure configurations in a full-factorial design set from a screening design set.

Algorithm 7 The Interpolation Approach: estimate unknown component values $\mathbf{V}_{\text{test}}$ for test configurations $\mathbf{V}_{\text{test}}$ in a full factorial set.

1: INPUT: $\mathbf{X}_{\text{test}}, \mathbf{X}_{\text{known}}, \mathbf{V}_{\text{known}}$
2: $N \leftarrow$ the number of components in the configurations of $\mathbf{X}_{\text{test}}$
3: **for** $i = 1, 2, 3, \cdots, N$ **do**
4: $\quad \mathbf{X}_p \leftarrow$ the i-th cascaded component of a configuration
5: $\quad \mathbf{X}_q \leftarrow$ the i-th cascaded component of the configurations of $\mathbf{X}_{\text{test}}$
6: $\quad \mathbf{V}_p \leftarrow$ component values corresponding to $\mathbf{X}_p$. it is obtainable from $\mathbf{V}_{\text{known}}$
7: $\quad \mathbf{V}_q \leftarrow function_{\text{interpolation}}(\mathbf{X}_p, \mathbf{V}_p, \mathbf{X}_q)$
8: $\quad \mathbf{V}_{\text{test}}(i) \leftarrow \mathbf{V}_q$
9: **end for**
10: OUTPUT: $\mathbf{V}_{\text{test}}$

In line 1, $\mathbf{X}_{\text{test}}, \mathbf{X}_{\text{known}}$, and $\mathbf{V}_{\text{known}}$ are a set of test configurations, a set of configurations with known component values, and a set of the known component values in $\mathbf{X}_{\text{known}}$, respectively. In line 7, a vector $\mathbf{V}_q$ is composed of interpolated component values on the components in $\mathbf{X}_q$ from the known component values in $\mathbf{V}_p$ on the components in $\mathbf{X}_p$ using Natural neighbor interpolation.

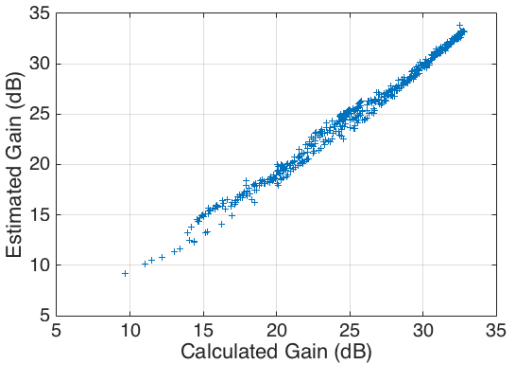

(a) Interpolated gain of an amplifier

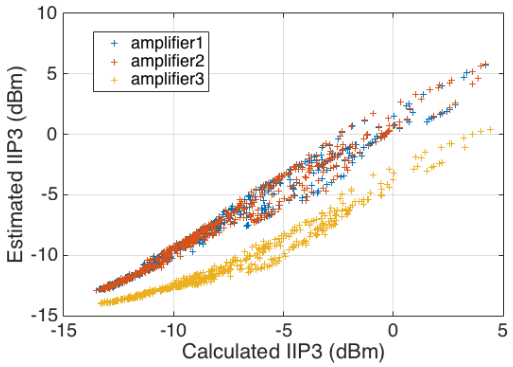

(b) Interpolated IIP_3 of an amplifier

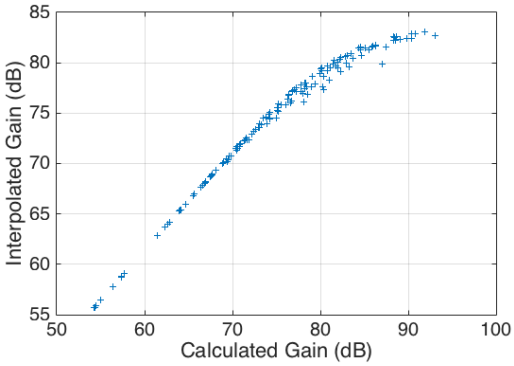

(c) Estimated gain of a configuration with three amplifiers using interpolated gain

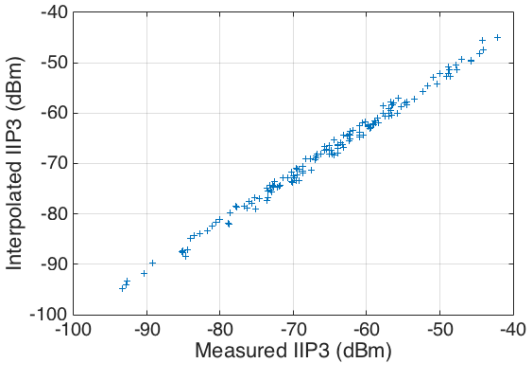

(d) Estimated IIP_3 of a configuration with three amplifiers using interpolated IIP3

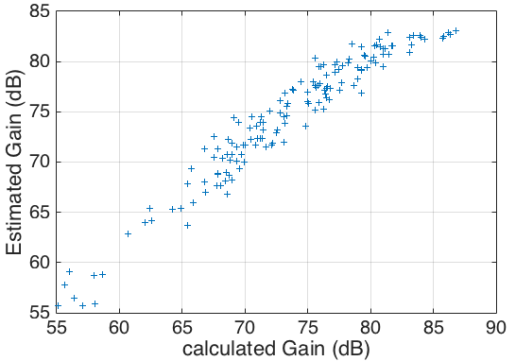

(e) Estimated gain of a configuration using simulation

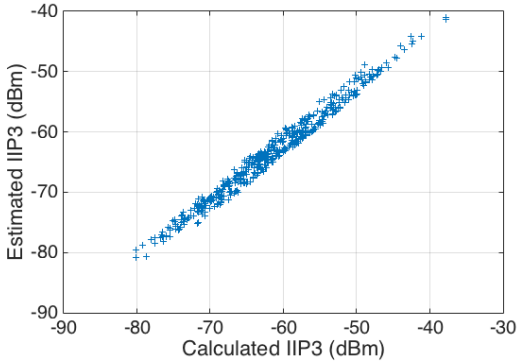

(f) Estimated IIP_3 of a configuration using simulation

Figure 4.8: Simulation Results of the Interpolation Method.

The gain and IIP_3 characteristics of amplifiers in the full factorial design set on the y-axis are obtained by applying the interpolation method to the corresponding estimators

of the screening design set. Figure 4.8a and 4.8b, which show gain and IIP_3 respectively on the y-axis, show close agreement with the true values on the x-axis.

The obtained RF impairment estimates using the interpolation method are applied to calculate the overall RF impairments of the configurations in the full factorial set using the formula (4.10), (4.11), (4.12). The calculated overall gain and IIP_3 of 150 configurations in a full factorial set on the y-axis are plotted against the true values on the x-axis in Figure 4.8c and 4.8d respectively while estimates of gain and IIP_3 obtained by simulation of the same configurations representing a full factorial set are plotted in Figure 4.8e and 4.8f. The results demonstrate that unknown RF impairments of the configurations in a full factorial design set are successfully obtained by applying the interpolation method.

Efficiency of the Design of RF Impairment Estimation for a Large-scale RF-FPGA

In this section, we discuss how the design of RF impairment estimation for a large-scale RF-FPGA improves the efficiency of RF impairment estimation. The designed DoE and interpolation methods are applied to measure RF impairment in a large-scale RF front-end of 63 bits from sample configuration data. In Table 4.2, the number of simulations (runs) and the required estimation time are calculated for three configuration sets: a full factorial design set, a screen designing set (of reconfiguring two MSBs of knobs) and a sample configuration set. The simulation time required for the estimation of gain is 41 seconds while IIP_3 is 42 seconds. The number of configurations to be simulated is about 10^{19}, 2.6×10^5, 384 in a full factorial design set, a screening design set and a sample configuration set, respectively. The total required simulation time is about 1.3×10^{13} years, 3×10^3 hours, and 4.4 hours, respectively. We found that while estimating RF impairments for a full-factorial or screening design set is costly and time-consuming, estimating RF impairments for sample configurations are powerful and cost-effective, as

shown in the Table 4.1. Thus, we verify that the design of RF impairment estimation for a large-scale RF-FPGA is important to utilize limited resources, such as time and power, for estimation.

Table 4.1: Comparison of Time Consumption for RF Impairment Estimation

RF Impairments	Gain	IIP_3
Simulation running time for a configuration	41 seconds	42 seconds
The number of simulations for full factorial designs	10^{19} runs	10^{19}
The number of simulations for screening designs (2 MSBs of components are reconfigured)	2.6×10^5 runs	2.6×10^5 runs
The number of simulations for sample configurations	384 runs	384 runs
Total simulation time for full factorial designs	1.3×10^{13} years	1.33×10^{13} years
Total simulation time for screening designs	3×10^3 hours	3.1×10^3 hours
Total simulation time for sample configurations	4.37 hours	4.45 hours

4.2 SINR Calculation in a Large-scale RF-FPGA

The Signal-to-Interference-and-Noise Ratio (SINR) of a configuration is calculated using (3.1) in Chapter 3. For the SINR calculation, we used the estimated RF impairments obtained by applying the DoE approach and the interpolation method as introduced in Section 4.1.2.

To compare the SINR calculation that uses estimated RF impairments to the SINR calculation using true component values, we considered two scenarios: (1) interference of the power -30 dBm at 20 MHz frequency offset from the signal of interest of -67 dBm, and (2) two interferences of the power -35 dBm at 150 MHz and 300 MHz frequency offset, respectively, from the signal of interest of -67 dBm. Figure 4.9 shows that the SINR calculated by using estimated values of RF impairments is in the reasonable range of the SINR calculated by using true values of RF impairments.

4.3 EAF-MR Optimization in a Large-scale RF-FPGA

We introduce the Environment-Adaptable Fast Multi-Resolution (EAF-MR) optimization designed for a large-scale RF-FPGA to adapt to the dynamic conditions in communication. We designed the EAF-MR optimization method by applying the EAF optimization that utilizes the SINR calculation to the Multi-Resolution (MR) optimization.

The MR optimization primarily has a similar structure as the Two-phase relaxation optimization in Section 3.2. In Phase I, the MR optimization iteratively finds the configuration of maximal SINR. In Phase II, starting from the found configuration, the MR optimization finds an optimal configuration that has the lowest power consumption satisfying the SNR specification for a given communication standard.

In order to improve the Two-phase relaxation optimization for a large-scale reconfig-

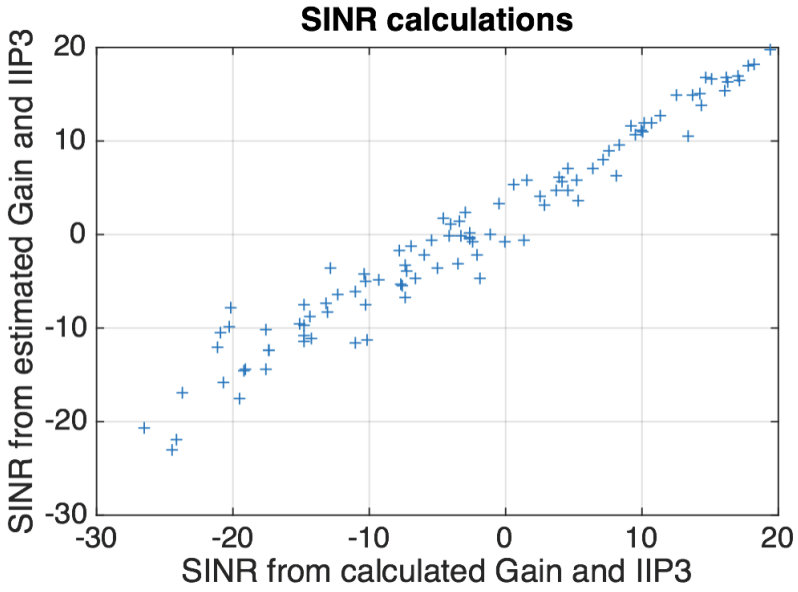

(a) Scenario 1: interference of the power -30 dBm at 20 MHz frequency offset from the signal of interest of -67 dBm.

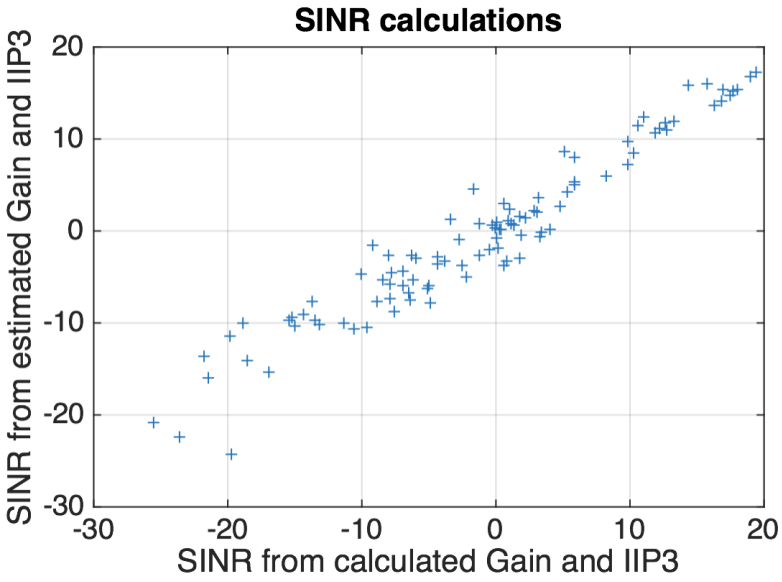

(b) Scenario 2: two interferences of the power -35 dBm at 150 MHz and 300 MHz frequency offset, respectively, from the signal of interest of -67 dBm.

Figure 4.9: SINR calculated using (3.1)

urable RF front-end, the MR optimization narrows down the search space into screening design sets of available configurations in a large-scale RF front-end. The size of screening design sets is determined by the number of active reconfiguration knob bits in all RF components. The fewer active bits of knobs, the more sparsely the characteristic values of the configurations in the screening design sets are distributed. The MR optimization tries to search for two types of configurations in the two phases, from small to large active bits. If there is no improvement for one cycle of iterations for all configurations, the iterative reconfiguration is stopped. The pseudocode of the MR algorithm is given in Algorithm 8.

In our EAF-MR optimization method, we applied the primary algorithmic structure of the MR optimization, and we utilized the calculated SINR in order to reduce the number of configurations to be simulated. When the SINR calculation of the configurations does not meet the pre-defined SINR threshold, the configurations are trimmed out in the list of configurations to be simulated. The pseudocode of the MR algorithm is given in Algorithm 9.

In Algorithm 8, $\mathbf{x}^{(current)}$, $\text{SNR}^{(current)}$, $\text{Power}^{(current)}$ represent a current configuration, the simulated SNR and power of the current configuration, respectively. $\text{nBit}_1{}^{(max)} = \text{nBit}_2{}^{(max)} = 4$ for our simulation setting. In line 2 to 17, a configuration with maximal simulated SNR (Phase I) is found. In line 7, a current knob $\text{K}^{(current)}$ is updated to the next available knob. In line 8, a list of configurations to be simulated is obtained by reconfiguring component values at the current knob $\text{K}^{(current)}$ of a current configuration $\mathbf{x}^{(current)}$. The resolution for the knob reconfiguration is given as $N_{\text{Resolution}}$. In line 9, $\text{SNR}(\mathbf{x})$ is obtained by simulating configurations of $\mathbf{x} \in \mathbf{X}$. In line 18 to 35, a configuration that has the lowest power while meeting a condition $\text{SNR}(\mathbf{x}) \geq \text{SNR}_{\text{Spec}}$ (Phase II) for $\mathbf{x} \in \mathbf{X}$ is found.

In Algorithm 9, $\mathbf{x}^{(current)}$, $\text{SNR}^{(current)}$, $\text{Power}^{(current)}$ represent a current configura-

Algorithm 8 Multi-Resolution Algorithm

INPUT: $\text{nBit}_1^{(max)}$, $\text{nBit}_2^{(max)}$
$\mathbf{x}^{(current)} \leftarrow \mathbf{x}^{(initial)}$, $\text{SNR}^{(current)} \leftarrow \text{SNR}^{(initial)}$, $\text{Power}^{(current)} \leftarrow \text{Power}^{(initial)}$
$\text{Power}(\mathbf{x}) \leftarrow$ power for $\forall \mathbf{x} \in \mathbf{X}$
for $N_{\text{Resolution}} = 1, 2, \cdots, \text{nBit}_1^{(max)}$ **do**
    $\text{K}^{(current)} \leftarrow \text{K}^{(initial)}$
    while (there has been recent updates on $\mathbf{x}^{(current)}$) **do**
        $\text{K}^{(current)} \leftarrow$ the next available knob component of $\mathbf{x}^{(current)}$
        $\mathbf{X} \leftarrow$ a set of configurations obtained by reconfiguring the component values with $N_{\text{Resolution}}$ bits control at $\text{K}^{(current)}$ of $\mathbf{x}^{(current)}$ while other components are fixed.
        $\text{SNR}(\mathbf{x}) \leftarrow$ simulated (or measured) SNR for $\forall \mathbf{x} \in \mathbf{X}$
        $\mathbf{x}^{(max)} \leftarrow \arg\max_{\mathbf{x} \in \mathbf{X}} \text{SNR}(\mathbf{x})$
        $\text{SNR}^{(max)} \leftarrow \text{SNR}(\mathbf{x}^{(max)})$
        if $\text{SNR}^{(max)} > \text{SNR}^{(current)}$ **then**
            $\mathbf{x}^{(current)} \leftarrow \mathbf{x}^{(max)}$, $\text{SNR}^{(current)} \leftarrow \text{SNR}^{(max)}$
            $\text{Power}^{(current)} \leftarrow \text{Power}(\mathbf{x}^{(current)})$
        end if
    end while
end for
for $N_{\text{Resolution}} = 1, 2, \cdots, \text{nBit}_2^{(max)}$ **do**
    $\text{K}^{(current)} \leftarrow \text{K}^{(initial)}$
    while (there has been recent updates on $\mathbf{x}^{(current)}$) **do**
        $\text{K}^{(current)} \leftarrow$ the next available knob component of $\mathbf{x}^{(current)}$
        $\mathbf{X} \leftarrow$ a set of configurations obtained by reconfiguring the values with $N_{\text{Resolution}}$ bits control at $\text{K}^{(current)}$ of $\mathbf{x}^{(current)}$ while other components are fixed.
        $\text{SNR}(\mathbf{x}) \leftarrow$ simulated (or measured) SNR for $\forall \mathbf{x} \in \mathbf{X}$
        if ($\text{K}^{(current)}$ is a knob component in a filter) **then**
            $\mathbf{x}^{(max)} \leftarrow \arg\max_{\mathbf{x} \in \mathbf{X}} \text{SNR}(\mathbf{x})$
            $\text{SNR}^{(max)} \leftarrow \text{SNR}(\mathbf{x}^{(max)})$
            if $\text{SNR}^{(max)} > \text{SNR}^{(current)}$ **then**
                $\mathbf{x}^{(current)} \leftarrow \mathbf{x}^{(max)}$, $\text{SNR}^{(current)} \leftarrow \text{SNR}^{(max)}$, $\text{Power}^{(current)} \leftarrow \text{Power}(\mathbf{x}^{(current)})$
            end if
        else if ($\text{K}^{(current)}$ is a knob component in an amplifier) **then**
            $\mathbf{x}^{(current)} \leftarrow \arg\min_{\mathbf{x} \in \mathbf{X} \text{ s.t. } \text{SNR}(\mathbf{x}) \geq \text{SNR}_{\text{Spec}}} \text{Power}(\mathbf{x})$
            $\text{SNR}^{(current)} \leftarrow \text{SNR}(\mathbf{x}^{(current)})$, $\text{Power}^{(current)} \leftarrow \text{Power}(\mathbf{x}^{(current)})$
        end if
    end while
end for
OUTPUT: $\mathbf{x}^{(current)}$, $\text{SNR}^{(current)}$, $\text{Power}^{(current)}$

Algorithm 9 EAF Multi-Resolution (EAF-MR) Algorithm

INPUT: $\text{nBit}^{(max)}$
$\mathbf{x}^{(current)} \leftarrow \mathbf{x}^{(initial)}$, $\text{SNR}^{(current)} \leftarrow \text{SNR}^{(initial)}$, $\text{Power}^{(current)} \leftarrow \text{Power}^{(initial)}$
$\text{K}^{(current)} \leftarrow \text{K}^{(initial)}$
$\mathbf{X} \leftarrow$ a set of configurations obtained by reconfiguring the values with $N_{\text{Resolution}}$ bits control at $\text{K}^{(current)}$ of $\mathbf{x}^{(current)}$ while other components are fixed.
$\text{SINR}^{(cal)}(\mathbf{x}) \leftarrow$ calculated SINR for $\forall \mathbf{x} \in \mathbf{X}$
$\text{Power}(\mathbf{x}) \leftarrow$ power for $\forall \mathbf{x} \in \mathbf{X}$
$\mathbf{x}^{(max)} \leftarrow \arg\max_{\mathbf{x} \in \mathbf{X}} \text{SINR}^{(cal)}(\mathbf{x})$
$\mathbf{x}^{(current)} \leftarrow \mathbf{x}^{(max)}$
$\text{SNR}^{(current)} \leftarrow$ simulated (or measured) SNR of $\mathbf{x}^{(current)}$
$\text{Power}^{(current)} \leftarrow \text{Power}(\mathbf{x}^{(current)})$
for $N_{Resolution} = 1, 2, \cdots, \text{nBit}^{(max)}$ **do**
    $\text{K}^{(current)} \leftarrow \text{K}^{(initial)}$
    while (there has been recent updates on $\mathbf{x}^{(current)}$) **do**
        $\text{K}^{(current)} \leftarrow$ the next available knob component of $\mathbf{x}^{(current)}$
        $\mathbf{X} \leftarrow$ a set of configurations obtained by reconfiguring the values with $N_{\text{Resolution}}$ bits control at $\text{K}^{(current)}$ of $\mathbf{x}^{(current)}$ while other components are fixed.
        $\mathbf{X}^{(pass)} \leftarrow \{\mathbf{x} \in \mathbf{X} | \text{SINR}^{(cal)}(\mathbf{x}) \geq \text{SINR}_{\text{Threshold}}\}$
        $\text{SNR}^{(pass)}(\mathbf{x}) \leftarrow$ simulated (or measured) SNR for $\forall \mathbf{x} \in \mathbf{X}^{(pass)}$
        if ($\text{K}^{(current)}$ is a knob component in a filter) **then**
            $\mathbf{x}^{(max)} \leftarrow \arg\max_{\mathbf{x} \in \mathbf{X}^{(pass)}} \text{SNR}(\mathbf{x})$
            $\text{SNR}^{(max)} \leftarrow \text{SNR}^{(pass)}(\mathbf{x}^{(max)})$
            if $\text{SNR}^{(max)} > \text{SNR}^{(current)}$ **then**
                $\mathbf{x}^{(current)} \leftarrow \mathbf{x}^{(max)}$, $\text{SNR}^{(current)} \leftarrow \text{SNR}^{(max)}$
                $\text{Power}^{(current)} \leftarrow \text{Power}(\mathbf{x}^{(current)})$
            end if
        else if ($\text{K}^{(current)}$ is a knob component in an amplifier) **then**
            for $\mathbf{x} \in \mathbf{X}^{(pass)}$ is selected in descending order of $\text{SNR}^{(pass)}(\mathbf{x})$ **do**
                if $\text{SNR}^{(pass)}(\mathbf{x}) \geq \text{SNR}_{\text{Spec}} \& \text{Power}(\mathbf{x}) < \text{Power}^{(current)}$ **then**
                    $\mathbf{x}^{(current)} \leftarrow \arg \min_{\mathbf{x} \in \mathbf{X} \text{ s.t. } \text{SNR}(\mathbf{x}) \geq \text{SNR}_{\text{Spec}}} \text{Power}(\mathbf{x})$
                    $\text{SNR}^{(current)} \leftarrow \text{SNR}(\mathbf{x}^{(current)})$
                    $\text{Power}^{(current)} \leftarrow \text{Power}(\mathbf{x}^{(current)})$
                    break
                end if
            end for
        end if
    end while
end for
OUTPUT: $\mathbf{x}^{(current)}$, $\text{SNR}^{(current)}$, $\text{Power}^{(current)}$

tion, the simulated SNR and power of the current configuration, respectively. In line 1, $\text{nBit}^{(max)} = 4$ for our simulation setting. In line 2 to 10, in order to find a configuration with maximal simulated SNR (Phase I), calculated SINR is utilized. In line 11 to 36, a configuration that has the lowest power while meeting a condition $\text{SNR} \geq \text{SNR}_{\text{Spec}}$ (Phase II) is found. In line 14, a current knob is moved to the next available knob and updated to $\text{K}^{(current)}$. In line 15, a list of configurations to be simulated is obtained by reconfiguring component values at the current knob $\text{K}^{(current)}$ of a current configuration $\mathbf{x}^{(current)}$. The resolution for the knob reconfiguration is given as $N_{\text{Resolution}}$.

4.3.1 Simulation

We finally demonstrate the performance of our EAF-MR optimization using a Matlab simulation.

Simulation Setting

We verified the performance of the designed EAF-MR optimization in a large-scale RF-FPGA (Figure 4.1) using Matlab Simulink shown in Figure 2.3 and 2.4. In the simulation, we used the communication standard IEEE 802.11g, and the required SNR specification is 11.5 dB. The transmitted signals have the bandwidth 20 MHz and the power -67 dBm. The RF-FPGA has 63 bits, which implies approximately 10^{19} configurations. There are two fixed RF filters, one fixed IF filter, and three 21 bit amplifiers. The power consumption range of all possible configurations is from 11.85 mW to 107.85 mW. We tested two optimization methods, MR and EAF-MR, on the scenario, which has one interferer of -30 dBm at 20 MHz frequency offset from the signal of interest.

Simulation Results

Table 4.2 shows the simulation results. While the MR optimization method took 2172 simulations for finding an optimal configuration, our EAF-MR optimization method required only two simulations. The EAF-MR optimization increases optimization efficiency since it is able to discard a large number of configurations whose calculated SINR does not satisfy the SNR specification. Both optimization methods found optimal configurations that satisfy the SNR specification (11.5 dB). The power consumption of the EAF-MR's optimal configuration is around 21 mW compared to around 12 mW (MR's optimal configuration). We found that the EAF-MR optimization is a trade-off between higher power consumption and the number of simulations.

Table 4.2: Simulation Results

Optimization Method	Power (mW)	SINR (dB)	Total Number of Simulations
Multi-Resolution Optimization	12.52	11.63	2172
MR-EAF Optimization	20.98	15.55	2

Table 4.3: Simulation Results of No. Simulations

Optimization Method	Phase I	Phase II	Total Number of Simulations
Multi-Resolution Optimization	816	1356	2172
MR-EAF Optimization	1	1	2

Therefore, we verified that our EAF-MR optimization method allows fast reconfiguration in dynamic communication environments, because it needs only a few reconfigurations to find the optimal one.

In this chapter, we have worked on the estimation process in order to utilize limited data resources for RF impairment estimation in a large-scale RF front-end. Using the estimated results, we designed the Environment-Adaptable Fast Multi-Resolution (EAF-MR) optimization. The EAF-MR optimization method utilizes calculated Signal-to-Interference-and-Noise Ratio (SINR) to reduce simulations in an optimization process in a large-scale RF front-end. Thus, our simulation set-up demonstrated the efficiency improvement of the EAF-MR optimization for a large-scale RF-FPGA.

Chapter 5

Conclusions and Future Works

In this thesis, we proposed the Environment-Adaptable Fast (EAF) optimization method for programming a reconfigurable RF front-end.

First, we studied estimation of gain, nonlinearity, phase noise, frequency offset, and noise figure for a reconfigurable RF front-end. Based on the signal model of baseband signals, we designed estimators of *Time-Invariant* (TI) RF impairments and *Time-Variant* (TV) RF impairments. TI RF impairments such as IIP_3 (nonlinearity) have fixed parameters and should be estimated when a reconfigurable RF front-end is manufactured. The estimators of gain and IIP_3 were designed using sinusoids with changed carrier frequencies. The estimators for phase noise spectrum were calculated by using the Interpolated Finite Impulse Response (IFIR) approach and the least mean square (LMS) adaptive algorithm. TV RF impairments have dynamic characteristic, and should be periodically estimated and updated. In order to utilize pilot signals, we designed TV RF impairment estimators invariant to other nuisance impairments. We derived a signal subspace model, and designed joint invariant estimators. Simulation results showed that the designed estimates of designed RF impairments are in an acceptable range.

Second, we designed the EAF optimization that speeds up an optimization process by

calculating the Signal-to-Interference-and-Noise Ratio (SINR) of possible configurations. The SINR calculation uses estimated RF impairments and a signal spectrum in a given communication environment. In the calculation, impairing signal power due to each of the RF impairments - phase noise, IIP_3, noise figure - was separately derived in terms of the power of the signal of interest and interference. Thus, real-time blocker information is reflected in SINR calculations. Also, we proposed the EAF optimization that quickly finds a configuration for a reconfigurable RF front-end. In Phase I, the EAF optimization directly finds a configuration of maximal SNR without any iterations using calculated SINR. In Phase II, SINR calculation was used to identify the configurations that likely do not meet a SINR specification and to narrow down the search space of configurations. Numerical experiments demonstrate that the EAF optimization method improves the efficiency of the optimization process for finding an optimal configuration. In particular, the EAF optimization method reduced the computational cost significantly, finding an optimal configuration after only five iterations instead of searching all possible configurations exhaustively.

Third, we investigated the application of the EAF optimization in a large-scale RF-FPGA. To estimate RF impairments in a large-scale RF front-end, we solved two main problems. First, we solved the saturation of nonlinear estimates due to a wide range of RF front-ends. To avoid the saturation problem, we obtained a formula for adjusting transmission power for an estimation procedure. Second, we solved a limited estimation resources problem. Because of a large number of configurations, it is not possible to directly measure and characterize the RF impairments of all possible configurations. We extended the estimation procedure to a large-scale RF-FPGA using the Design of Experiments (DoE) approach and the Interpolation method. Finally, we designed a EAF Multi-Resolution (EAF-MR) optimization method in which the EAF optimization method

was applied to a Multi-Resolution (MR) optimization. Simulation results showed that our EAF-MR optimization requires only two iterations while MR optimization takes more than 2000 iterations. There is a trade off between efficiency and local optimum. However, as an optimal configuration exists, finding a global optimum is not necessary. The main focus of our research is attaining low computational cost (fast convergence) in optimization for a real-time application. Therefore, using this algorithm, reconfigurable RF front-ends can move forward to a reliable multi-standard platform for the needs of future communication systems.

In the future, we want to investigate spectral strategies that help to prune the space of RF configurations to be explored ("search space") and rules to automatically rank preferred RF configurations. In order to narrow down the search space, we plan to study the heuristic rules that are applicable using the reconfigurability of filters and local oscillators (LOs). While reconfiguring filters and LOs, we assume that the characteristics of RF components (e.g. filters' center frequency and bandwidth) and also the signal spectrum are accessible. When a blocker appears, in order to improve communication quality, in addition to the choice of filters, etc, we can also change either radio frequency (RF) or intermediate frequency (IF) of the RF system based on the blocker information in the signal spectrum. For example, the blocker signal can be effectively eliminated if it is placed on the stopband of a notch filter in the frequency domain. In order to satisfy this condition, the IF of a reconfigurable RF front-end can be changed by reconfiguring LOs considering the characteristics of the notch filter. The heuristic strategies for reconfiguring filters and LOs will help a reconfigurable RF front-end improve the speed of an optimization process for In-theater mode.

Appendices

Appendix A

Reconfigurable RF front-end vs. Wide-band RF front-end

To demonstrate the usefulness of a reconfigurable RF front-end, we compared it to a fixed wide-band front-end using the Simulink platform of Mathworks, which was augmented with the SimRF toolbox.

A.1 Simulation Setting

The simulated scenario was as follows. The signal of interest is a IEEE 802.11g WLAN signal with a carrier frequency 2.4 GHz and bandwidth of 20 MHz, received at -75 dBm. We added to the signal two interferers located at 2.475 GHz and 2.550 GHz. The first interferer is received at -30 dBm while the second interferer is received at powers ranging from -100 dBm to 0 dBm. (This range is selected because blockers of power up to 0 dBm may be observed above 500 MHz, according to the survey in [18].)

In the scenario, we compare two architectures: a fixed wide-band RF front-end and a reconfigurable RF front-end. The fixed wide-band RF front-end has a digital attenuator

whose gain can be varied from -0.5 dB to -31.5 dB. The reconfigurable RF front-end has 9747 configurations, one of which is optimal. Each of two narrow-band RF filters is reconfigured by 19 configurations, all with various center frequency, filter order and bandwidth [10]. Each of three amplifiers is reconfigured by three configurations, using different gain, nonlinearity and noise figure. After down-conversion by the mixer, both the systems use an IF filter to remove out-of-band interference, followed by a digital SDR to do digital channel selection and digital down-conversion into baseband. These steps are typical of an SDR such as the USRP. A baseband 802.11g demodulator then decodes the obtained baseband signal.

A.2 Simulation Results

The maximal possible SINR, obtained by varying the attenuator (fixed RF case) or by choosing the optimal configuration (reconfigurable RF case), is plotted against the second interferer's power in Figure A.1. We observe that the SINR of the fixed wide-band RF front-end drops dramatically to reach 0 dB when the interferer power is higher than -50 dBm. However, the reconfigurable RF front-end has an SNR of 18.8 dB even with very high interferer power up to 0 dBm. Note that the interferers are located far from the signal channel of interest. These interferers are removed by the IF filter that precedes the SDR in both cases. The degradation in performance in the fixed RF case is mainly due to the non-linearity of the RF front-end, which causes inter-modulation interference to appear in the channel of interest. While the inter-modulation interference is typically weak, it becomes significant when the interferer power is large, as has previously happened in the fixed front-end case. On the other hand, the reconfigurable front-end allows for judicious use of RF filters, so that the interference will likely to be attenuated sufficiently when it

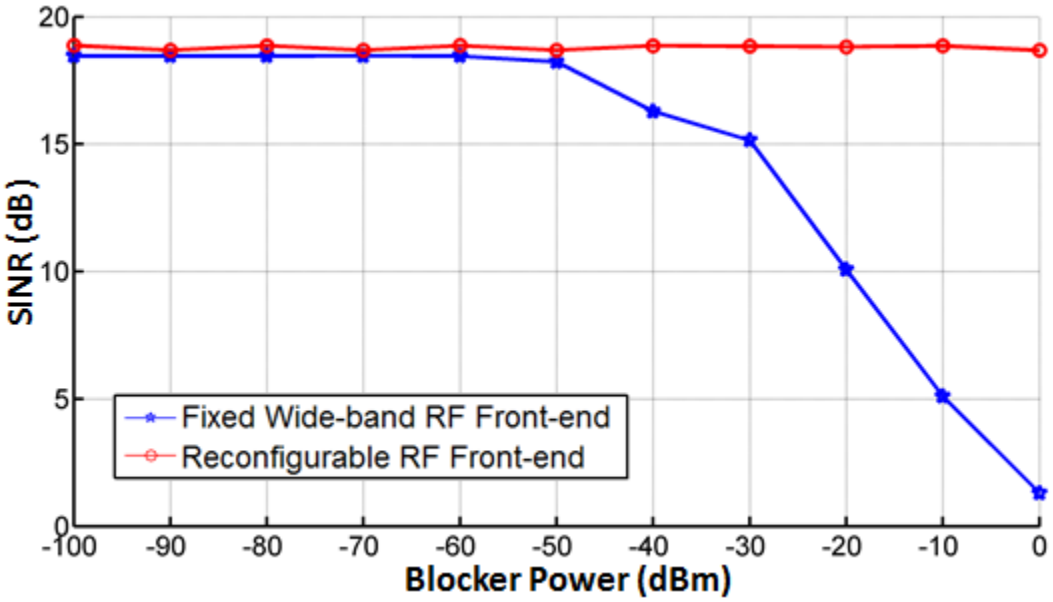

Figure A.1: SINR (dB) vs blocker power (dBm) of a fixed wide-band RF front-end (blue) and ra econfigurable RF front-end (red).

cause significant inter-modulation in the subsequent RF chain. Thus, we conclude that the reconfigurable RF front-end, properly adapted, can outperform the fixed wide-band RF front-end when there are high power interferers, due to non-linearity induced inter-modulation. Therefore, the reconfigurable RF front-end can be used to obtain a reliable multi-standard platform.

Appendix B

Factory and In-theater Modes

In order to solve this optimization problem efficiently in real-time, we define three stages in Factory mode and Theater mode as below:

B.1 Factory Mode

B.1.1 Profiling Stage

When manufacturing a reconfigurable RF front-end in a factory, a *Configuration Profile Table* is built in order to provide information about all possible configurations in the reconfigurable RF front-end. For example, we decide if a configuration can operate for a signal of interest based on the filter bandwidth and carrier frequency for each configuration in the table. Also, the Configuration Profile Table provides the third-order intercept point (IP3), a metric of non-linearity of RF components, needs to be given to predict the inter-modulation effect of blockers in our algorithm.

B.2 In-theater Mode

B.2.1 Exploring Stage

In contrast to Factory mode, a reconfigurable RF front-end updates real-time information for practical use. In particular, we periodically update a *Real-Time Table* using estimated SINR, based on the Configuration Profile Table created in Factory mode and the blocker distribution given by *Spectrum Analyzer* .

B.2.2 Optimizing Stage

We run an environment-adaptable and fast optimization algorithm to find the optimal configuration $\mathbf{x}_t^{(opt)}$ of a reconfigurable RF front-end at time t. In order to improve its efficiency, the algorithm reflects real-time information of communication environments using the Real-Time Table as well as the Configuration Profile Table.

Appendix C

Phase Noise Impairments

In this section, we show how strong interference can interact with phase noise. We investigate the phase noise effect with and without interference using the IEEE 802.11a and IEEE 802.11b transceivers as examples. Simulations are performed using Matlab Simulink with the SimRF block set. In Table 2.1, we note that the IEEE 802.11a and IEEE 802.11b standards require -102 dBc/Hz and -101 dBc/Hz phase noise, respectively, at 1 MHz frequency offset.

In Figure C.2 and C.3, we plotted two scenarios in order to observe phase noise impairments.

In the first scenario, we assumed that there is no interference and only the signal of interest is presented. The signal of interest was -65 dBm for the IEEE 802.11a standard and -76 dBm for the IEEE 802.11b standard, as shown in Figure C.1. The signal-only case is depicted as the green curves in Figure C.2 and C.3. Because of other impairments such as nonlinearity, the simulated SINR curve converges to a constant in the low phase noise range. Otherwise, SINR decreases by 3 dB as phase noise increases by 3 dB in simulated SINR, and also in calculated SINR, which is derived from (3.3) in Section 3.1.

In the second scenario, we assumed that interference exists in addition to the signal of

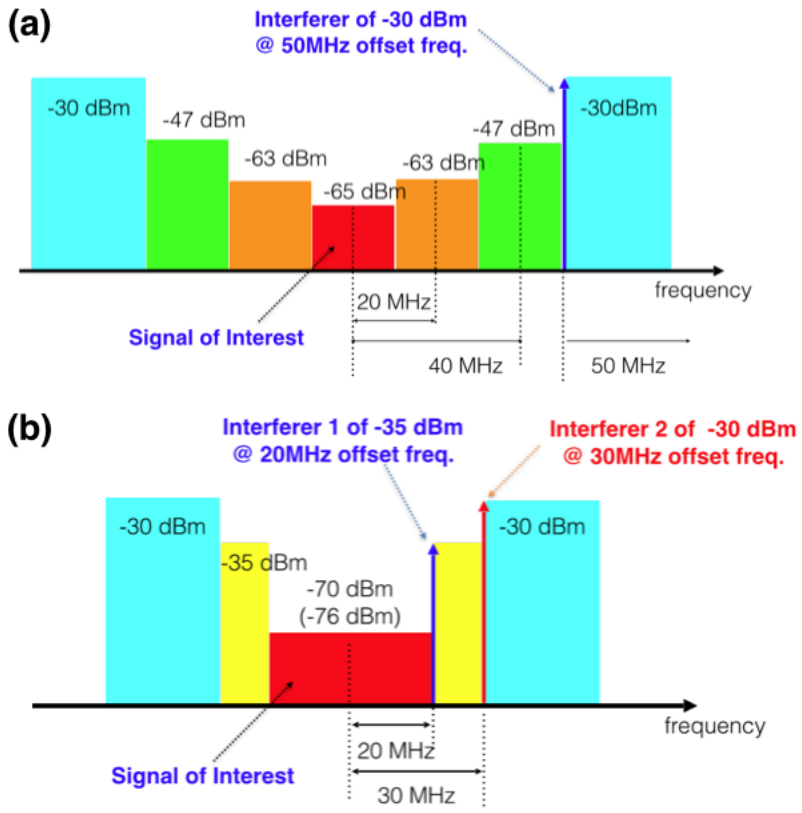

Figure C.1: Blocking Mask- (a) the IEEE 802.11a standard (b) the IEEE 802.11b standard [2].

interest. In our scenario, we had the interferer of -30 dBm at 50 MHz frequency offset, the worst possible case specified by the blocking mask in the IEEE 802.11a as shown in Figure C.1 (a). For the IEEE 802.11b, we consider the two possible scenarios specified by the standard: the interferer of -35 dBm at 20 MHz frequency offset and the interferer of -30 dBm at 30 MHz frequency offset.

For IEEE 802.11a, Figure C.2 shows that the required phase noise is -108 dBc/Hz at 1MHz frequency offset, which is more stringent than -102 dBc/Hz from Brandolini's study [2] as specified in Table 2.1. This phenomenon is explained as follows: the impairing signal caused by phase noise and the signal of interest in (3.3) and the impairing

signal by phase noise and interference in (3.4) have almost the same value. The summed signal is about 3 dB higher than either one of the impairing signals. Then, the SINR of the impairing signals' sum is about 3 dB lower than that found in Brandolini's study. Thus, SINR was impacted by the signal of interest and also by interference (in Section 3.1). This shows the need to derive a more accurate formula for SINR when there is phase noise and interference.

For IEEE 802.11b, our simulation results in Figure C.3 show that phase noise requirement is about -102 dBc/Hz, which is consistent with -101 dBc/Hz in Table 2.1. As expected, the SINR with interference is much lower than the SINR without interference because interference effect dominates phase noise.

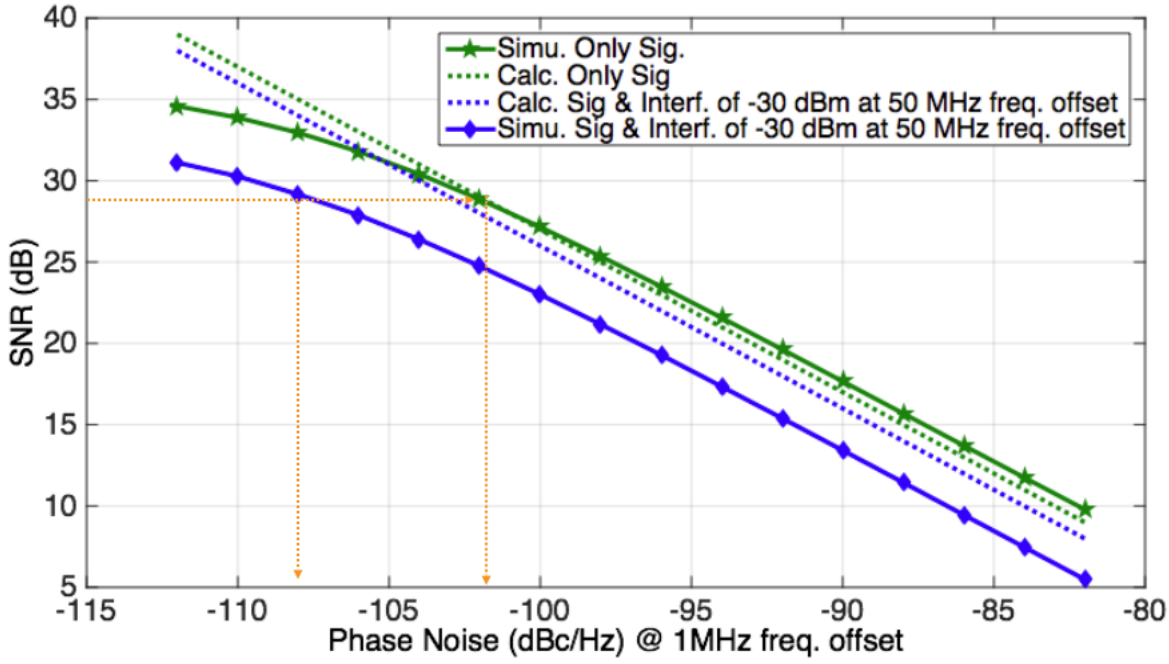

Figure C.2: SINR (dB) vs. Phase Noise (dBc/Hz at 1MHz frequency offset) for the IEEE 802.11a with the SINR requirement of 29 dB.

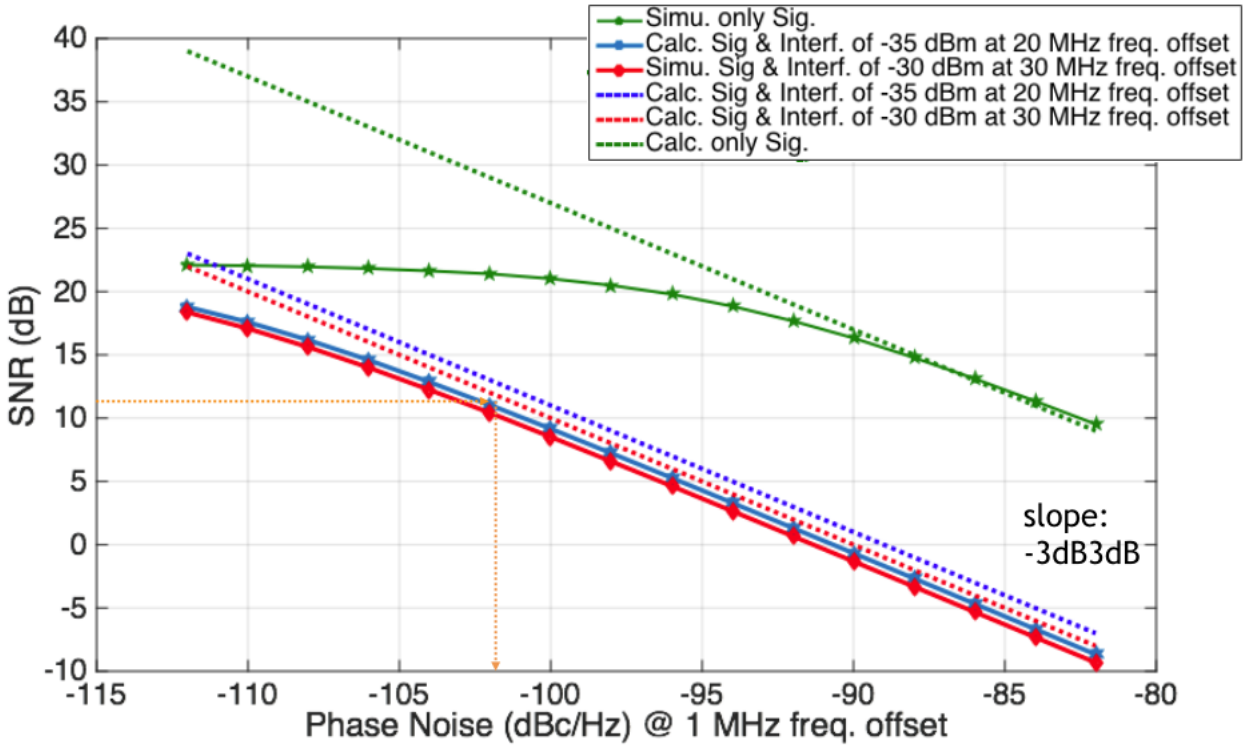

Figure C.3: SINR (dB) vs. Phase Noise (dBc/Hz at 1MHz frequency offset) for the IEEE 802.11b with the SINR requirement of 14.5 dB.

Bibliography

[1] Lauri Anttila, Dani Korpi, Ville Syrjala, and Mikko Valkama. Cancellation of power amplifier induced nonlinear self-interference in full-duplex transceivers. In *Signals, Systems and Computers, 2013 Asilomar Conference on*, pages 1193–1198. IEEE, 2013. 2.2.1

[2] Massimo Brandolini, Paolo Rossi, Danilo Manstretta, and Francesco Svelto. Toward multistandard mobile terminals-fully integrated receivers requirements and architectures. *Microwave Theory and Techniques, IEEE Transactions on*, 53(3):1026–1038, 2005. (document), 2, 2.1, C.1, C

[3] Bruce E Carey-Smith, Paul A Warr, Phill R Rogers, Mark A Beach, and Geoffrey S Hilton. Flexible frequency discrimination subsystems for reconfigurable radio front ends. *EURASIP Journal on wireless communications and networking*, 2005(3):354–363, 2005. 1.1

[4] DARPA. Radio Frequency-Field Programmable Gate Arrays (RF-FPGA), November 2011. URL `https://www.fbo.gov/?tab=documents&tabmode=form&subtab=core&tabid=cd49cf41f5df4f860046cb3a9bdfe8d9`. 1.1

[5] Wataru Doi. Spectrum analyzer, October 31 2000. US Patent 6,140,809. 3.1.4

[6] Minhee Jun, Rohit Negi, Jun Tao, Ying-Chih Wang, Shihui Yin, Tamal Mukherjee, Xin Li, and Larry Pileggi. Environment-adaptable efficient optimization for programming of reconfigurable radio frequency (RF) receivers. In *Military Communications Conference (MILCOM), 2014 IEEE*, pages 1459–1465. IEEE, 2014. 2.1.1, 2.1.1, 3.2.2, 3.1, 3.2

[7] Minhee Jun, Rohit Negi, Ying-Chih Wang, Tamal Mukherjee, Xin Li, Jun Tao, and Larry Pileggi. Joint invariant estimation of RF impairments for reconfigurable radio frequency (RF) front-end. In *Globecom Workshops (GC Wkshps), 2014*, pages 954–959. IEEE, 2014. 2.2, 2.2.2

[8] Minhee Jun, Rohit Negi, Shihui Yin, Fa Wang, Megha Sunny, Tamal Mukherjee, and Xin Li. Phase noise impairment and environment-adaptable fast (EAF) optimization for programming of reconfigurable radio frequency (RF) receivers. In *Globecom, 2015 (to appear in)*. IEEE, 2015. 2.1.2

[9] N Jeremy Kasdin. Discrete simulation of colored noise and stochastic processes and $1/f^{\alpha}$ power law noise generation. *Proceedings of the IEEE*, 83(5):802–827, 1995. 2.1.2

[10] Juseop Lee, Eric J. Naglich, Hjalti H. Sigmarsson, D. Peroulis, and W.J. Chappell. Tunable inter-resonator coupling structure with positive and negative values and its application to the field-programmable filter array (fpfa). *Microwave Theory and Techniques, IEEE Transactions on*, 59(12):3389–3400, Dec 2011. ISSN 0018-9480. doi: 10.1109/TMTT.2011.2171711. A.1

[11] Paul H Moose. A technique for orthogonal frequency division multiplexing frequency offset correction. *Communications, IEEE Transactions on*, 42(10):2908–2914, 1994. 2

[12] Praween Kumar Nishad and P Singh. Carrier frequency offset estimation in ofdm systems. In *Information & Communication Technologies (ICT), 2013 IEEE Conference on*, pages 885–889. IEEE, 2013. 2.2.1

[13] Jongsun Park, Khurram Muhammad, and Kaushik Roy. Efficient modeling of $1/f^{\alpha}$ noise using multirate process. *Computer-Aided Design of Integrated Circuits and Systems, IEEE Transactions on*, 25(7):1247–1256, 2006. 2.1.2, 2.1.2

[14] Ettus Research. Bandwidth capability of USRP devices, Apr 2014. URL `http://www.ettus.com/kb/detail/usrp-bandwidth`, `https://www.ettus.com/product/details/WBX120`. 1.1

[15] Louis L. Scharf. *Statistical signal processing: detection, estimation, and time series analysis*. Addison-Wesley Pub. Co., 1 edition edition, 1991. 2.1.2, 2.2.2

[16] Louis L Scharf and Benjamin Friedlander. Matched subspace detectors. *Signal Processing, IEEE Transactions on*, 42(8):2146–2157, 1994. 2.2.2

[17] T. C W Schenk and E.R. Fledderus. Rf impairments in high-rate wireless systems - understanding the impact of tx/rx-asymmetry. In *Communications, Control and Signal Processing, 2008. ISCCSP 2008. 3rd International Symposium on*, pages 117–122, March 2008. doi: 10.1109/ISCCSP.2008.4537203. 2

[18] Christer Svensson. The blocker challenge when implementing software defined radio receiver rf frontends. *Analog Integrated Circuits and Signal Processing*, 64(2): 81–89, 2010. A.1

[19] Jun Tao, Ying-Chih Wang, Minhee Jun, Xin Li, R. Negi, T. Mukherjee, and L.T. Pileggi. Toward efficient programming of reconfigurable radio frequency (RF) receivers. In *Design Automation Conference (ASP-DAC), 2014 19th Asia and South Pacific*, pages 256–261, Jan 2014. doi: 10.1109/ASPDAC.2014.6742899. 1.2, 3.2.1,

3.2.2, 3.1, 3.2

[20] Parishwad P Vaidyanathan. Multirate digital filters, filter banks, polyphase networks, and applications: A tutorial. *Proceedings of the IEEE*, 78(1):56–93, 1990. 2.1.2